Fiber-Optic Sensors for Weigh-In-Motion Application

by

Majid Mehdikhani

Thesis submitted to the Faculty of the

Virginia Polytechnic Institute and State University

in partial fulfillment of the requirements for the degree of

Master of Science

in

Electrical Engineering

APPROVED:

Dr. A. Safaai-Jazi, Chairman

Dr. S. A. Ardekani

Dr. T. C. Poon

September 1989

Blacksburg, Virginia

Fiber-Optic Sensors for Weigh-In-Motion Application

by

Majid Mehdikhani

Dr. A. Safaai-Jazi, Chairman

Electrical Engineering

(ABSTRACT)

Automated techniques to acquire weight and traffic data are indispensable to effective management and maintenance of the vast network of highways. Weigh-In-Motion (WIM) systems have the potential to greatly reduce the cost and improve the accuracy associated with weight data collection.

The existing WIM systems utilizing piezoelectric cables have been shown to result in rather large random errors of up to 12% and need to be installed at permanent sites. In addition, the exponential decay of the output signal of the piezoelectric cable with time can cause complications in signal processing and possibly further errors.

In this thesis, a fiber-optic sensor is proposed which measures the pressure generated by the weight of a vehicle. The system consists of a pneumatic tube filled with an incompressible fluid, a rubber pad embedding the tube, a diaphragm to convert pressure into displacement, and an optical displacement sensor. A prototype of the proposed sensor is designed, manufactured and tested in the laboratory.

Both piezoelectric cable and the optical sensor are tested under varying load-frequencies. It is shown that the piezoelectric cable sensor shows considerable dependence on the load frequency, whereas the response of the proposed system is much less frequency dependent and, unlike the piezoelectric cable has a waveform similar to that of the

applied load. This latter property can significantly reduce the difficulties associated with signal processing. Besides, the linearity of response over the range of loads applied is better than that of the piezoelectric cable. This implies that the proposed fiber-optic sensor with its high rate of accuracy can be implemented under conditions where piezoelectric sensor does not deliver accurate results. For example, when equally loaded axles at different vehicle speeds and axle configurations are used.

Acknowledgements

I wish to thank Dr. A. Safaai-Jazi, my major advisor, and Dr. S. A. Ardekani whose many comments, suggestions, and criticisms have been invaluable and are greatly appreciated. Additionally, I would like also to thank Dr. T. C. Poon for serving on my committee, and Ahmad Razvan, and Mehran Elahi for their assistance in conducting the experiments. I am also deeply indebted to my parents for their ever lasting encouragement and support throughout my education.

Table of Contents

List of Illustrations

List of Tables

Chapter 1. Introduction

1.1. Background

To properly plan for the maintenance and management of the nation's vast network of highways, large quantities of traffic data are required. As a minimum, data must be collected on the number, type, weight, and speed of vehicles on the highways. To date, the need exists for automated techniques to acquire such data economically and accurately. Currently, for example, most truck weight data are obtained statically at truck weigh stations. These facilities are not only costly to equip and operate, but also are fixed in location and often operating hours. Consequently, the weight data obtained tend to underestimate the number of over-weight trucks that manage to bypass the stations.

In this regard, Weigh-In-Motion (WIM) systems have the potential to greatly reduce the cost and improve the accuracy associated with weight data collection. Early WIM

systems generally consisted of a number of strain gauges mounted on the under-side of bridge girders or under flush-type platforms. The major drawback of such systems has been their high cost, typically ranging from $50,000 to $200,000 per unit.

Almost from the inception of WIM systems in the early 1950's, efforts have been concentrated on developing low cost WIM sensors. As part of these efforts, the use of piezoelectric cables has subsequently reduced the equipment cost. The states of Iowa and Minnesota, for example, have each installed a piezoelectric WIM system for an approximate equipment cost of $5000 per lane [1]. Colorado [2] and Texas [3,4] have also experimented with this technology.

Despite their relatively low cost and small systematic errors, piezoelectric sensors have been shown to result in rather large random errors for individual axles. Researchers in Canada reported piezoelectric cable accuracy of 6% to 12% as compared to the dynamic axle load measurements by an instrumented vehicle [5]. The experiments in Canada involved three vehicle speeds, two levels of tire pressure, and two suspension types. Studies in Texas involving some 800 trucks weighed both statically and by using the piezoelectric WIM system showed overall random errors of up to 9% [6]. Studies in Iowa involving 456 trucks reported overall random errors of up to 12% [7] for a WIM system installed in a rigid (portland concrete) pavement. Similar experiments designed for a flexible (asphalt concrete) pavement case in Minnesota were not carried out due to problems relating to the sensor installation, electronics and pavement behavior [7].

Although installation problems such as those encountered in Minnesota can eventually be resolved, the magnitude of random errors in other studies carried out is rather large. Such errors arise, among others, due to the internal geometry and bending

characteristics of the cable, the design of sensor mounting, the roadway surface profile upstream of sensor installation [8].

The use of a fiber-optic sensor as a replacement for the piezoelectric cable in WIM systems is highly promising. Fiber-optic sensors have the potential to alleviate a number of error sources associated with the piezoelectric sensors. Furthermore, they offer a potentially lower equipment, installation, and maintenance cost.

Fiber-optic sensing technique have attracted considerable attention in recent years. Several factors contribute to the rapid growth of fiber optic sensor technology, including low cost, small size, high sensitivity, and immunity from electromagnetic interference (EMI). Among the various advantages offered by fiber-optic sensors, low cost and immunity from electromagnetic interference are particularly appealing to vehicle weighing and traffic control applications. The present systems used for weighing-in-motion are not only expensive, but also suffer from relatively large errors.

1.2. Approach

The main problem of vehicle weighing is, in fact, pressure sensing. Various techniques for pressure sensing using fiber-optic technology have been studied in the past decade [9-13]. These techniques are based on variations of one or more of transmission properties of the light. The simplest pressure sensor operates based on the amplitude modulation of the light. Amplitude sensors are easy to construct, inexpensive and function reliably in harsh environments. For applications where moderate sensitivities are sufficient, amplitude sensors are suitable candidates. In situations where highly accurate data and high sensitivities are required Mach-Zehnder interferometric phase

sensors may be utilized [14]. Phase sensors, however, have complicated structures and are expensive. Another promising pressure sensor is based on modal interference in a few-mode fiber which offers sensitivities between those of amplitude and phase sensors [15].

For vehicle weighing applications, an amplitude sensor is a reasonable choice because it is low cost and can offer the desired accuracy. An important advantage of amplitude sensors is that the power is much less sensitive to random temperature variations than the phase sensors. This aspect is of considerable importance in designing reliable optical WIM sensors. Fiber-optic pressure sensing can be implemented using a variety of techniques. The sensing mechanism may be either intrinsic in which case the pressure affects the fiber directly, or extrinsic where the modulation of light takes place outside the fiber. Here an extrinsic approach is adopted. The pressure generated by the weight of a vehicle upon pressing on a fluid-filled pneumatic tube is converted to displacement by means of a diaphragm. The deflection of diaphragm modulates the light.

A prototype pressure sensor, operating based on an extrinsic fiber-optic displacement sensing technique, is designed, analyzed, and evaluated experimentally. In Chapter 2 the principle of operation of piezoelectric cable is reviewed. To compare the performance of the piezoelectric cable with that of the proposed sensor, a series of tests are carried out. Fiber-optic techniques for pressure sensing are addressed in Chapter 3. Advantages and disadvantages of various techniques are pointed out and ways of improving the sensitivity are discussed. Chapter 4 gives the details of the design of the proposed sensor. Optical and electronics aspects of the design are addressed. Mechanical design considerations, experimental results, and evaluation of the performance of the proposed

sensor are discussed in Chapter 5. Concluding remarks and suggestions for further work are summarized in Chapter 6.

Chapter 2. Piezoelectric sensor

The principle of operation of piezoelectric cable is briefly described. To compare the performance of piezoelectric cable under varying load magnitudes and frequencies with that of the proposed sensor, a series of experiments are carried out. The output signal of the cable is obtained for thirty load-frequency combinations. The experimental results indicate that the peak voltage and the decay time of the output signal are frequency dependent. Besides, the cable response is not linear over a wide range of loads. This implies that in current piezoelectric WIM systems, equally loaded axles could generate different output signals depending on the vehicle speed and axle configuration.

2.1. Principle of operation

A piezoelectric cable is essentially a coaxial cable in which the region between the inner and outer conductors is filled with a piezoelectric material in the form of a compressed powder. The piezoelectric material acts as a dielectric for the coaxial cable. The material is poled by a radial electric field generated between the inner and outer conductors, thus allowing a piezoelectric response to radial stress [16]. Piezoelectricity is a property of some materials that manifests itself by the generation of electrical charges of opposite polarity when they are subjected to a mechanical stress. It arises because of an interaction between Coulomb forces and the elastic restoring forces [17]. The amount of charge induced depends upon the change of the applied pressure. In other words, the output voltage of a piezoelectric cable, which is proportional to the charge induced, depends upon the time derivative of the pressure and is not proportional to the pressure itself. Thus, a constant pressure gives rise to an output voltage which decays with time.

2.2. Experimental Design

The piezoelectric sensor used consists of a piezoelectric cable embedded in epoxied resin and housed in an aluminum frame of 20x20*mm* cross section and is about 3.5 meters long. The sensor was installed onto the stationary upper plate of an MTS (Material Test Systems) machine. The piezoelectric cable was firmly supported by six wooden columns along its length, in order to dampen undesired vibrations. Load was applied from below through a metallic support plate of about 64.5cm^2 (10 in^2) in contact area. Figure 1 shows the block diagram of the experimental set up.

A 20-Kip MTS machine was used and five levels of load were applied (1 to 4 Kips in 1-Kip increments). Each load was applied at different frequencies of 0.25, 0.5, 1, 2, 5, and 10 Hz. Table 1 summarizes all load-frequency combinations. Ten cycles of a square wave were applied at each load-frequency combination (see Table 1). A square wave was used so that the sensor was loaded during half of each cycle. For example, for a load at 2 Hz frequency, each cycle is 0.5 seconds long (0.5-second period) and the sensor is loaded for 0.25 seconds in each cycle. The MTS was interfaced to an oscilloscope. The input and output signals were monitored simultaneously and photographed following each load application.

2.3. Performance under varying load frequencies

An aspect of the accuracy of the piezoelecric sensor, particularly not addressed in the past, is its sensitivity to the frequency of the load applied. Axle loads were simulated by an MTS loading cell applying five different loads at six different frequencies. The output signal of the piezoelectric cable was obtained for each load-frequency combination. The output waveforms were photographed for all cases, but in order to limit the number of figures, only waveforms corresponding to 0.25 Hz, 2 Hz, and 10 Hz frequencies are presented here. Figures 2-5 illustrate these waveforms for loads 1, 2, 3, 4 Kips, respectively. Each figure shows two waveforms; the upper waveform represents the piezoelectric cable output signal, while the lower one corresponds to the MTS load signal, which hereafter is referred to as the input signal. In all tests, the load has been applied on a $64.5 cm^2$ ($10\ in^2$) contact area.

An examination of the output waveforms indicates that the initial application of the load induces a voltage which rises rapidly from zero to a maximum value, then decays in an exponential manner. After the load is removed, the output voltage undergoes another change reaching a negative peak which also decays exponentially with time. It is thus evident that the response of the piezoelectric cable depends upon the time derivative of the applied load, i.e., df/dt. This behavior is more clearly demonstrated at lower frequencies as seen in Figures 2.a-5.a, which correspond to 0.25 Hz frequency. At this frequency the load waveform is nearly a square wave. At higher frequencies, e.g., 10 Hz in Figures 2.c-5.c, the input waveforms are not clean square waves, but the output signals exhibit peaks at instants of application and removal of the load, just as in the case of low frequency loads. In general, however, variations of the output signal with time for the high frequency loads is more complex, exhibiting an oscillatory behavior during the decay period. These oscillations may be attributed to residual vibrations of the cable at higher load frequencies. This difference in decay time of the induced voltage at low versus high frequencies could be an additional source of error in piezoelectric WIM systems.

Figure 6 is a plot of the output voltage versus the load applied. Figure 7 is the best-fit regression line through the data points, namely $y = -12.6 + 16.4x$, where y is the output signal (mV) and x is the applied load (Kips). The coefficient of determination (R^2) is 92.9% indicating a fairly linear relation between the applied load and the output signal. More importantly, the t-values for the intercept and slope are -4.77 and 17.01, respectively, with 22 degrees of freedom. These values correspond to levels of significance (p-values) of 0.00009208 and 0.00000000, respectively. It can therefore be concluded that, while the intercept is effectively zero, the p-values suggest that the slope is significantly different from zero. Figure 6 compares variations of the peak output

voltage versus load at six different frequencies. It appears that the output signal is not independent of the applied frequency. For example, a 4-Kip load applied at a 10 Hz frequency generates the same voltage as a 3-Kip load at 0.25 Hz frequency (Figure 6). This simply implies that, two vehicles with different axial loads and speeds result in the same output response. Moreover, the cable response is not piecewise linear for loads greater than 3-Kips. This nonlinearity becomes more significant at higher frequencies. It must be noted that in Fig. 6, a decline in voltage is experienced upon the application of a 4-Kip load at frequencies under 10 Hz. This decline is due to unexpected failure of the steel support structure holding the piezoelectric cable during testing and not an inherent characteristic of the piezoelectric cable.

The dependency of the output signals on load frequency is statistically verified through two-sample t-tests, the results of which are shown in Table 2. The output signal under each load frequency is tested against any other frequency for statistical significance of differences. The corresponding p-values are tabulated in Table 2, showing for example that the output signals at 1 Hz are different from those at 0.25 Hz at 91% level of significance or higher. Of course, the higher the p-values, the less significant the observed differences will be. In this regard, the matrix entries in Table 2 must be compared to the respective matrix entries for the fiber-optics WIM sensor results presented in Chapter 5. Further evidence of the output sensitivity to load frequency is obtained through examining the coefficient of variation of the output signals for each level of loading. Using the data in Table 1, coefficients of variation of 34%, 8%, 20%, and 14% are obtained for loads of 1 to 4 Kips, respectively. While the variation is smallest for 2-Kips load (8%), in all other cases the values are over 10% indicating errors due to frequency.

In summary, the piezoelectric sensor response over a wide range of applied loads displays rather large seemingly random errors with frequency of the applied load. These would make the correlation of the cable response to the axle weight of the vehicle a difficult task, since the voltage signal received for equally loaded axles would be different depending on the vehicle speed and axle configuration.

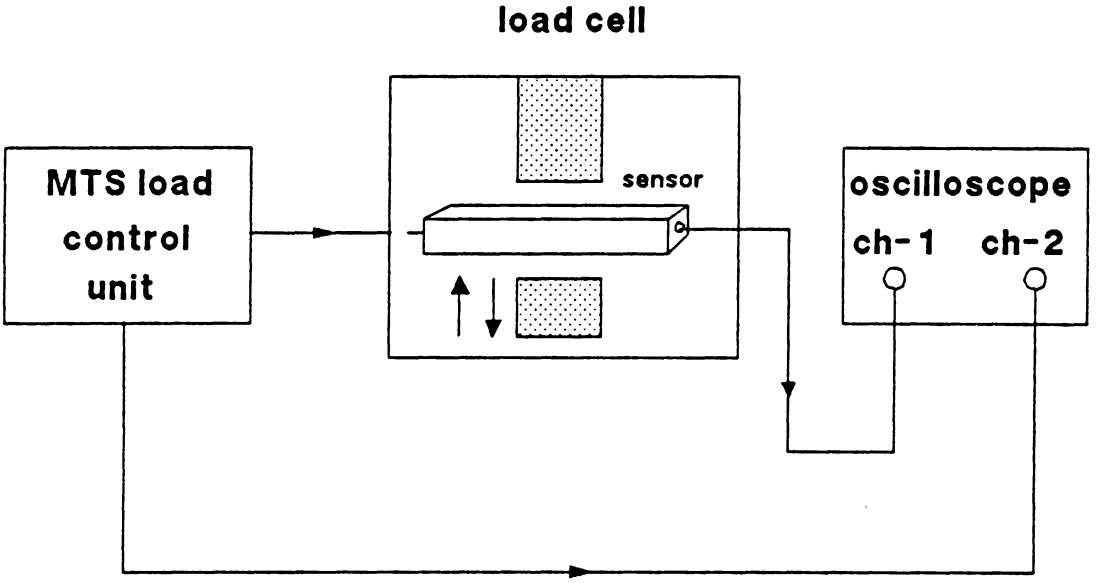

Figure 1. Block diagram of the experimental set up for the piezoelectric sensor.

(a)

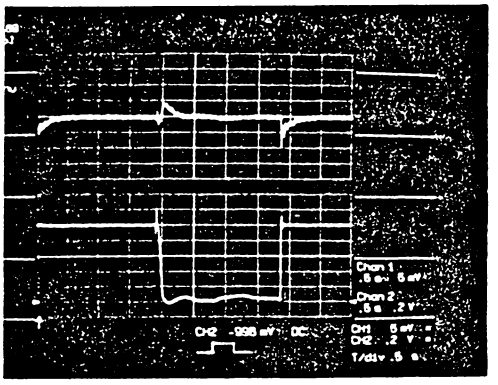

(b)

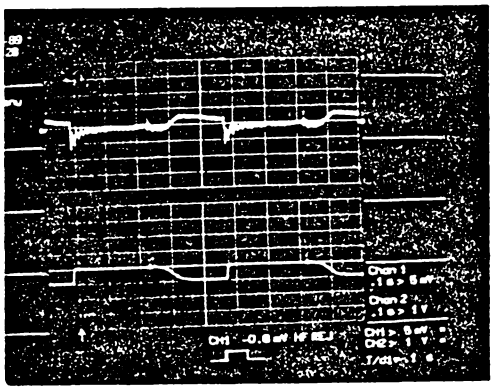

(c)

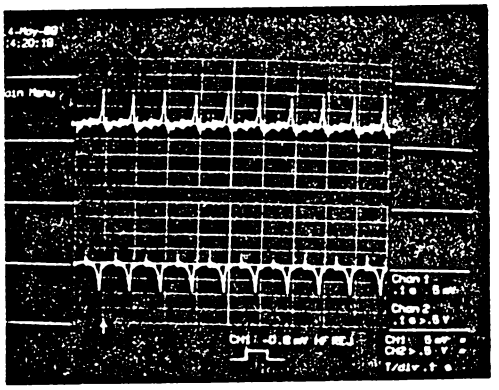

Figure 2. Response of piezoelectric sensor for 1 Kip load at frequency (a) 0.25 Hz, (b) 2 Hz, and (c) 10 Hz.

(a)

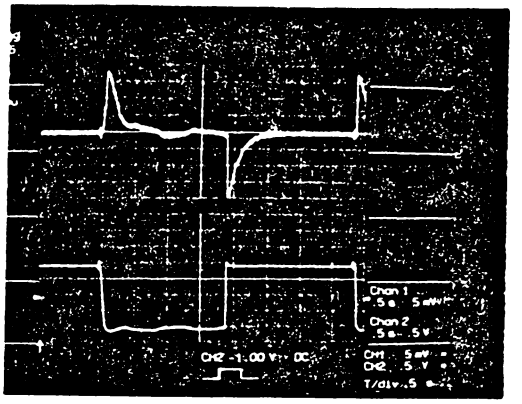

(b)

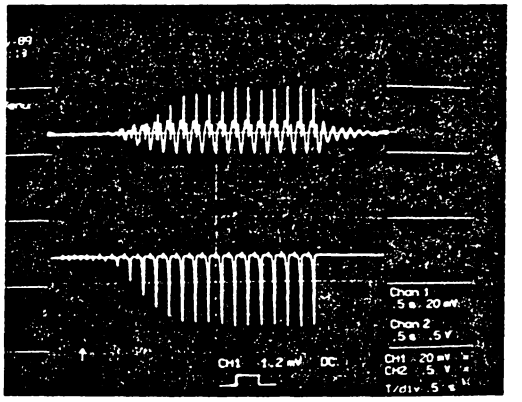

(c)

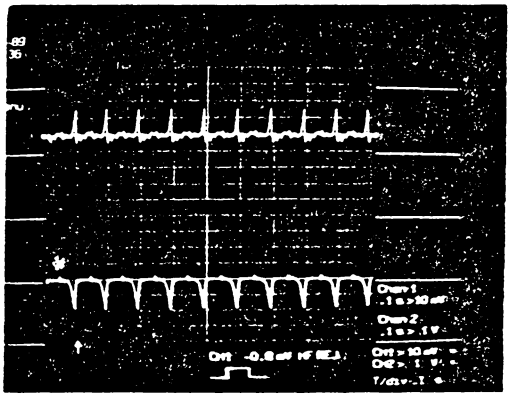

Figure 3. Response of piezoelectric sensor for 2 Kips load at frequency (a) 0.25 Hz, (b) 5 Hz, and (c) 10 Hz.

(a)

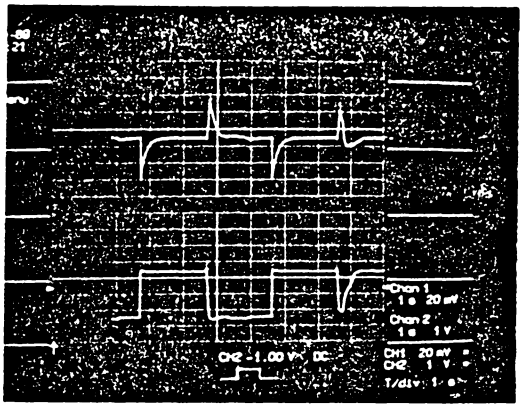

(b)

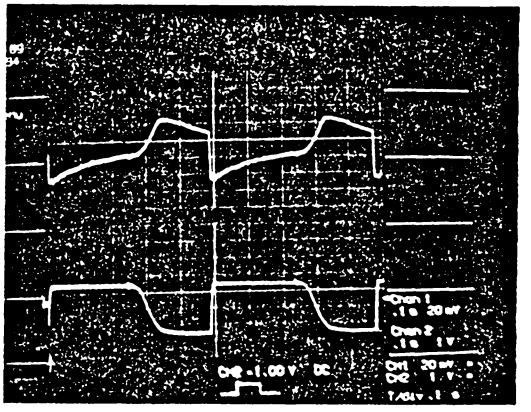

(c)

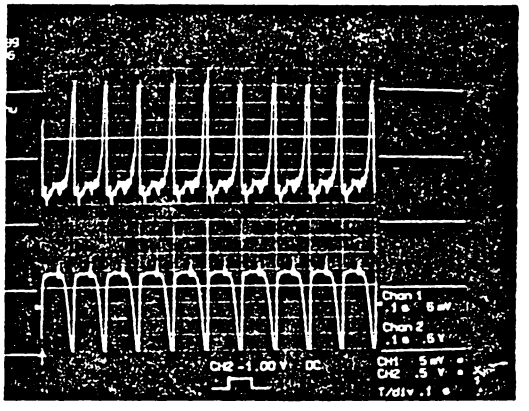

Figure 4. Response of piezoelectric sensor for 3 Kips load at frequency (a) 0.25 Hz, (b) 2 Hz, and (c) 10 Hz.

(a)

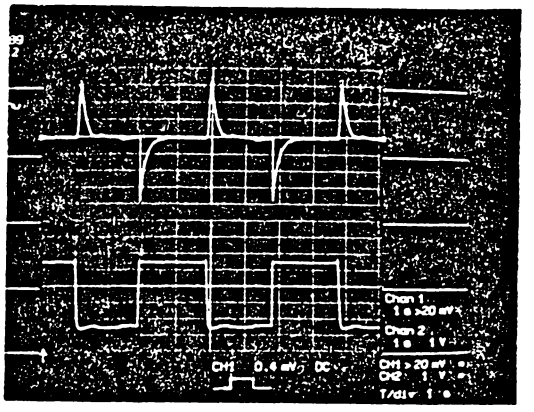

(b)

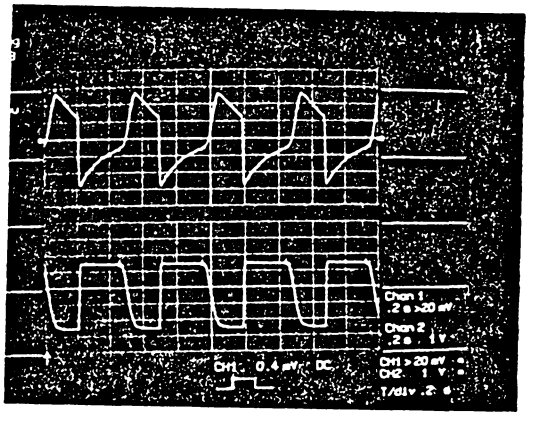

(c)

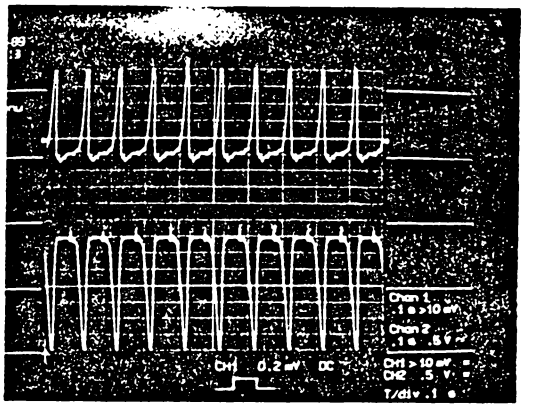

Figure 5. Response of piezoelectric sensor for 4 Kips load at frequency (a) 0.25 Hz, (b) 2 Hz, and (c) 10 Hz.

Table 1. Experimental data for piezoelectric sensor.

	Induced peak voltage(mV) @ frequency of					
Load(Kips)	0.25 Hz	0.5 Hz	1.0 Hz	2.0 Hz	5.0 Hz	10.0 Hz
1.0	4.0	5.0	5.0	3.0	5.0	8.0
2.0	19.0	20.0	20.0	20.0	20.0	16.0
3.0	40.0	25.0	33.0	45.0	36.0	30.0
4.0	60.0	58.0	57.0	52.0	59.0	40.0
Mean	35.0	31.2	31.2	33.6	33.2	32.4
St. dev	23.22	21.51	19.85	21.20	21.25	23.43

Table 2. P-values for 2-sample t-test on piezoelectric sensor experimental data.

	0.5 Hz	1.0 Hz	2.0 Hz	5.0 Hz	10.0 Hz
0.25 Hz	0.83	0.91	0.97	0.97	0.64
0.5 Hz		0.92	0.86	0.86	0.80
1.0 Hz			0.94	0.94	0.71
2.0 Hz				1.0	0.65
5.0 Hz					0.66

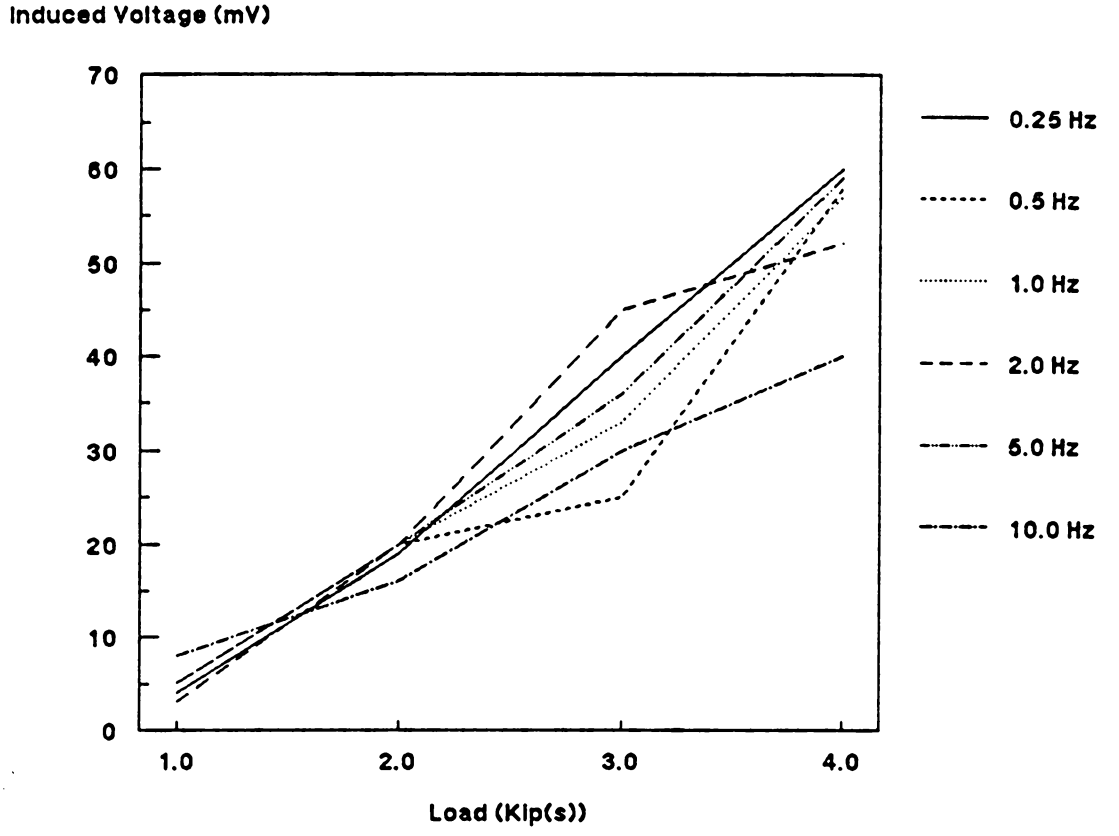

Figure 6. Variation of piezoelectric cable output voltage versus load at different frequencies.

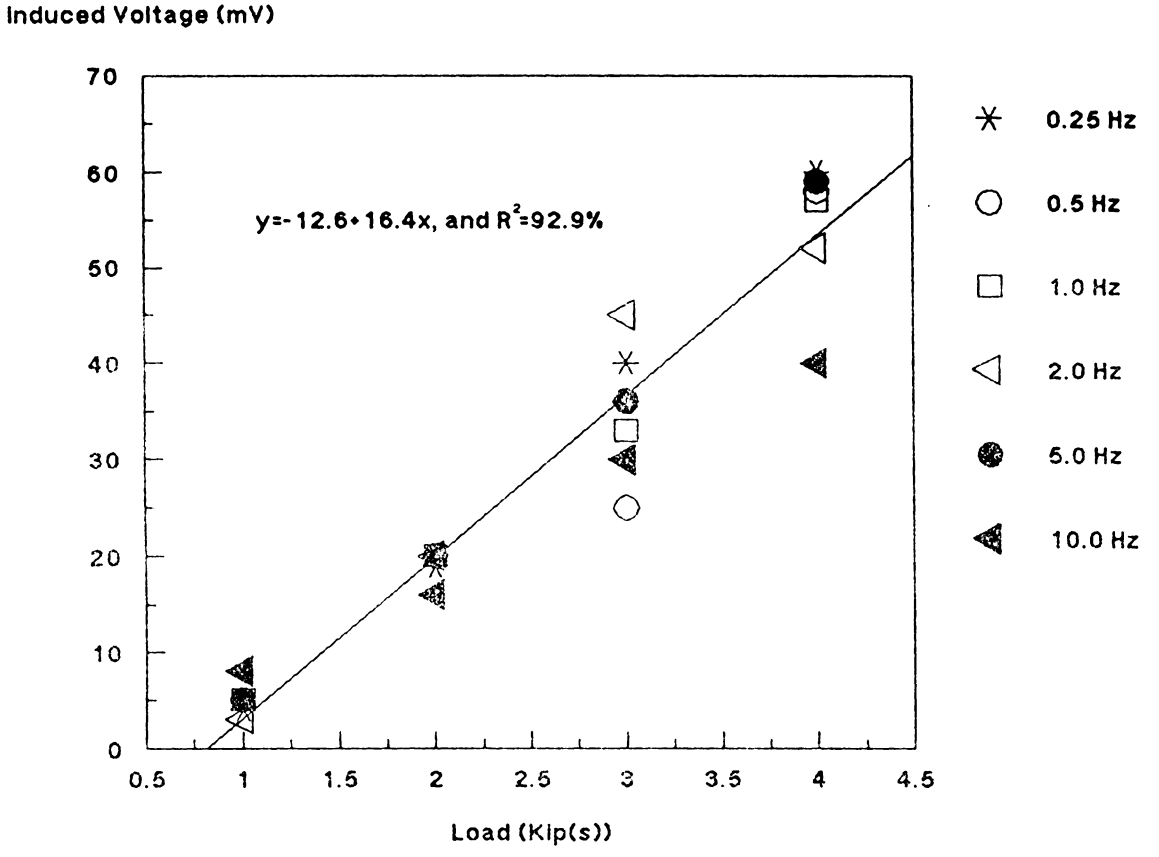

Figure 7. Linear regression of experimental data for piezoelectric sensor at varying frequencies of applied load.

Chapter 3. Fiber-optic techniques for pressure sensing

This chapter examines various fiber-optic techniques for the measurement of pressure. The principles of operation of fiber-optic pressure sensors are discussed. Sensing techniques based on the modulation of amplitude or phase of light are addressed. Both intrinsic and extrinsic sensing mechanisms are reviewed. Various options pertinent to weighing-in-motion systems are evaluated and a design is proposed taking into account cost, accuracy, and durability of the sensor.

3.1. Principles of operation

A light beam is associated with a number of physical properties including amplitude (intensity), phase, wavelength (color), polarization, and mode of propagation. In the absence of any external disturbance, the properties of light remain unchanged. If an external disturbance such as pressure, stress, strain, temperature, electric field, etc perturbs the transmission medium in some way, one or more properties of light will change. The amount of change is a measure of the external disturbance.

In this work, the external disturbance is the pressure generated by the weight of a vehicle. Pressure can perturb the transmission medium in many different ways. If the transmission medium in contact with the pressure region is an optical fiber, perturbations would commonly include bends, microbends, refractive index change, induced anisotropy, and dimension changes, all of which affect the transmission properties of the light propagating in the fiber. Geometrical changes such as bends and microbends affect the intensity considerably, whereas perturbations in the refractive index bring about significant changes in the phase. The loss of power, resulting from bends and microbends, is due to the conversion of the guided modes to radiation modes. Variations of the phase, on the other hand, result from the elasto-optic effect as well as changes in the fiber dimensions.

When the transmission medium is air, the disturbance can indirectly alter the properties of light. For example, pressure can move a blocking element and cause the light to be only partially transmitted. Variations in the transmitted or reflected power are then related to the applied pressure.

3.2. Intrinsic sensing techniques

As discussed earlier, the parameters specifying the light propagating in an optical fiber can be altered if subjected to direct contact with external perturbations such as pressure, strain, etc. These changes can then be correlated to the measurand of interest. Applicability of this idea, further subdivides the optical sensing techniques into two categories, where each category operates on substantially different principles and has different areas of application. Both categories employ sensors which operate based on the modulated transmission/reflection losses. First, the group where the intensity pattern set up by the light launched into a mechanically supported fiber is altered due to direct contact with the physical quantity being measured (intrinsic). These concepts are integrated into various sensing techniques.

Often it is desired to acquire information about a parameter of interest such as pressure and to transport the information to a convenient location due to the nature of application or the environmental set of conditions imposed. This concept makes up the characteristics of the second group. In latter, modulation of light parameters is correlated to the measurand indirectly (extrinsic). For example, pressure can be converted into displacement which in turn can change the power of the reflected or transmitted light. This concept makes up the foundation of optical sensing techniques employed for weighing-in-motion and is further elaborated upon in sub-sections 3.3.1 and 3.3.2.

3.2.1. Amplitude sensing technique

This technique is based on the idea that, the external disturbance modulates the insertion loss of the optical fiber. If two corrugated plates, known as deformers sandwich an optical fiber along its axis as shown in Fig. 8, and the plates are displaced with respect to one another due to the introduction of an external pressure, a spatial periodic fiber deformation will be developed. This deformation in turn will cause mode coupling. Light is redistributed among newly developed modes, and at the same time couples light from guided to radiation modes. The amount of power coupled to radiation modes which escapes the fiber is an excess loss. It has been shown [18] that for microbend deformations, mode coupling of light occurs between every two modes whose propagation constants K_1 and K_2 satisfy the condition $K_1 - K_2 = \pm (2\pi/\Lambda)$, where Λ is the mechanical wavelength of the periodic microbend disturbance. By closely monitoring the optical power at the output end of the fiber, one can determine the amount of the applied pressure. Microbend sensors offer sufficient sensitivities and are suitable candidates for the measurements of relatively small pressures. Since optical fibers can not sustain high shear stresses, microbend sensors are not favored for WIM applications.

3.2.2. Interferometric sensing technique

This technique incorporates the phase modulation of optical signal to measure the external disturbance. It can be implemented using a variety of schemes. An arrangement commonly used in fiber-optic sensing is the Mach-Zehnder interferometer shown schematically in Fig. 9. This interferometer consists of essentially two arms, one serving as sensing arm and another as reference arm. The light signal is divided between the two

arms using a 3-dB coupler. The external disturbance affects only the sensing arm and causes the light signal propagating in this arm to undergo a phase change. The signals of the two arms are then combined using a second 3-dB coupler. The two signal interfere, as a result the phase difference between them is converted to an amplitude change which can be easily monitored and measured by means of a detection circuit.

Interferometric sensors offer very high sensitivities and are useful for measuring small disturbances. A major drawback of these sensors is their sensitivity to random temperature variations. To eliminate this problem, sophisticated control systems are required which make the sensor complicated and expensive. In view of the fact that in WIM systems pressures are not small and the cost needs to be kept as low as possible, an interferometric type sensor is not a suitable choice.

3.3. Extrinsic sensing techniques

In an extrinsic fiber-optic sensing scheme, the external disturbance does not affect the fiber directly. That is, the light is modulated outside the fiber. The role of the fiber in such sensor is to transmit light to and from the sensing region. Extrinsic fiber-optic sensors are of particular interest in low cost WIM systems. Here two sensing schemes based on reflection and transmission of light are described.

3.3.1. Reflection-based method

Figure 10 illustrates the schematic diagram of a pressure sensor based on the external modulation of light intensity. Light is coupled into a multimode fiber from an LED (Light Emitting Diode) or a laser diode. The length of the fiber depends upon the needs of a specific application. The fiber is followed by a 3-dB coupler which divides the power into halves. One of the coupler's output fiber is attached to a GRIN (GRaded-INdex) lens which collimates and expands the light beam, while the other output fiber is immersed in an index matching fluid which absorbs the light. Parallel to the GRIN lens face, a mirror is mounted which can move up and down. The motion of the mirror is controlled by the pressure to be measured. In the absence of any pressure, the mirror does not block the light exiting the GRIN lens, thus no reflection takes place. By increasing the pressure, the mirror is displaced in the vertical direction, thus causing a portion of light to be reflected back into the GRIN lens. The reflected light is focused (by the focusing action of the GRIN lens) on to the fiber, passes through the coupler and half of its power eventually reaches the detector. The detector's output voltage is proportional to the reflected power which in turn is dependent upon the applied pressure. The GRIN lens helps the system to respond more linearly by collimating the light beam.

The concept of reflection-based pressure sensor may also be implemented using horizontal motion for the reflecting element. The operation of this sensor, shown in Fig. 11, is similar to that described above. Here, the amount of reflected light coupled back into the fiber depends upon the gap between the reflecting surface and the fiber end. The amount of light coupled back into the fiber is a nonlinear function of the gap, thus a nonlinear pressure sensor.

3.3.2. Transmission-based method

In the reflection-based scheme described above, twice the power is divided into halves, thus always a 6-dB loss. Besides, the fiber-GRIN lens connection needs very careful alignment to avoid further loss of power. The power efficiency can be improved by a factor of 6-dB by eliminating the coupler and using a separate channel for the detector as illustrated in Fig. 12. The principle of operation of this sensor is the same as that of Fig. 10, with the difference that, the detector measures the power of the transmitted light. If the sensing region can accommodate the source, detector, and associated electronics, fibers and GRIN lenses may also be eliminated, and the sensor head assembly reduces to that shown in Fig. 13.

3.3.3. Use of gratings to improve sensitivity

Gratings can be used to increase sensitivity for both reflection-based and transmission-based sensors. Here the use of gratings in transmission-based sensors is described. Gratings are parallel and equally spaced strips deposited on transparent glass substrates (or mirrors) as shown in Fig. 14a.

The material used in the construction of gratings should be highly absorptive (black). One grating is placed in front of the GRIN lens (or LED if GRIN lens is not used), and another one replaces the blocking element in Fig. 13. When the strips of the gratings overlap completely, maximum transmission takes place (Fig. 14b). When the grating attached to the diaphragm is displaced, the path of light is partially blocked and transmission is reduced (Fig. 14c). For a displacement equal to one half the grating

period, the path is completely blocked and transmission is reduced to zero (Fig. 14d). This qualitative analysis, of course does not take into account diffraction by the strips edges. It is clear that the sensitivity can be increased by reducing the grating period. It should be noted that, the response of the sensor becomes periodic and there is a 3-dB power loss since, in the absence of any displacement when the gratings are assumed to have a perfect overlap, only half the power is transmitted.

In summary, the relative merits of six different sensing techniques have been evaluated and compared. The six sensing techniques studied here, are seen to offer different rates of accuracy, power consumption, and parts count. Since the objective of this endeavor was to study the feasibility of developing a low-cost Weigh-In-Motion pressure sensor as a possible replacement for the presently implemented piezoelectric Weigh-In-Motion sensor, then a design based on transmission-based sensing techniques (see Fig. 13) is justified. They are relatively low cost, and the entire unit will be packaged into a small unit. More importantly, they offer high rate of accuracies.

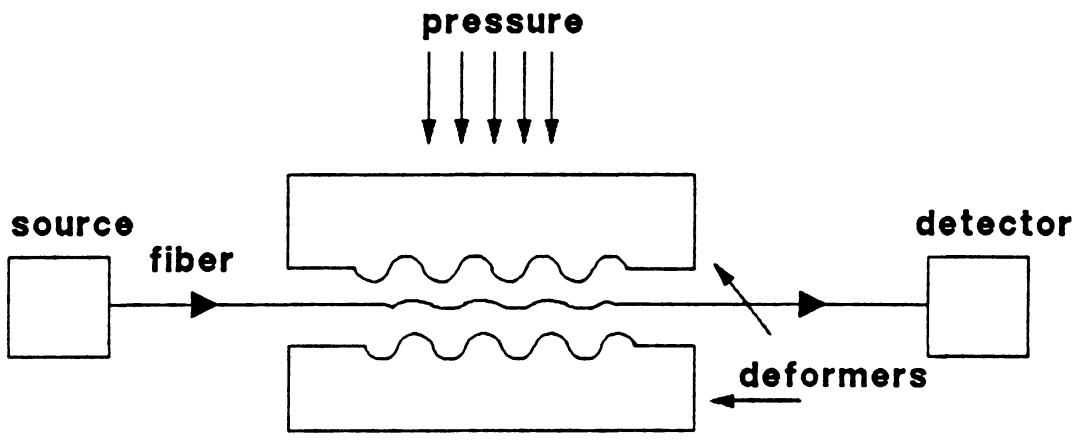

Figure 8. Schematic diagram of microbend sensor.

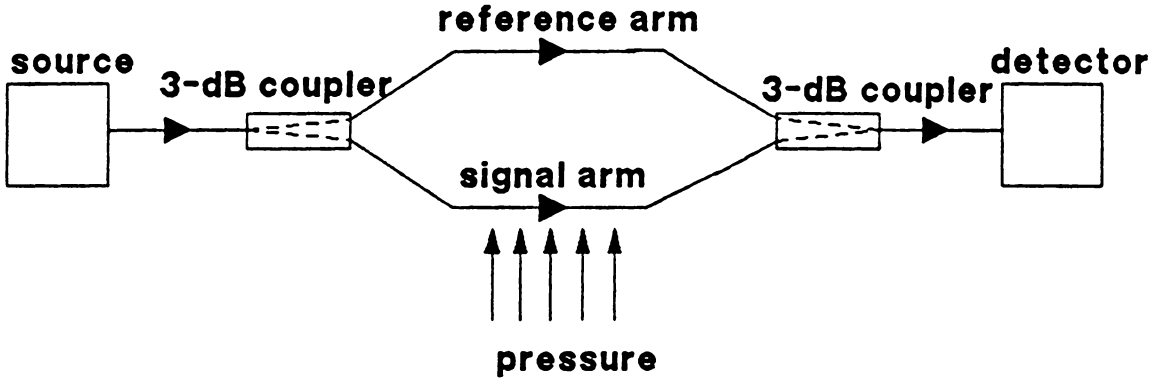

Figure 9. Schematic diagram of a Mach-Zehnder interferometric sensor.

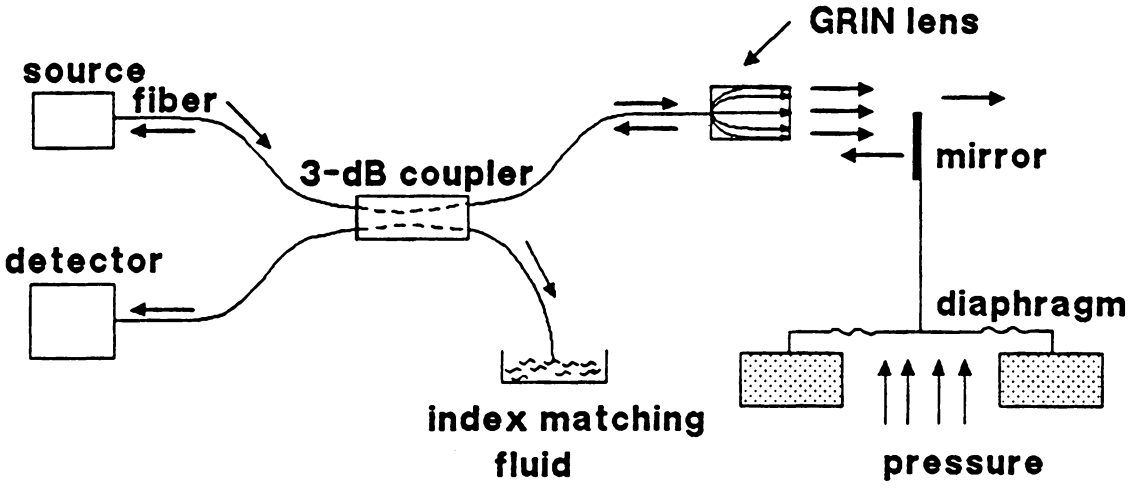

Figure 10. Schematic diagram of a reflection-based pressure sensor.

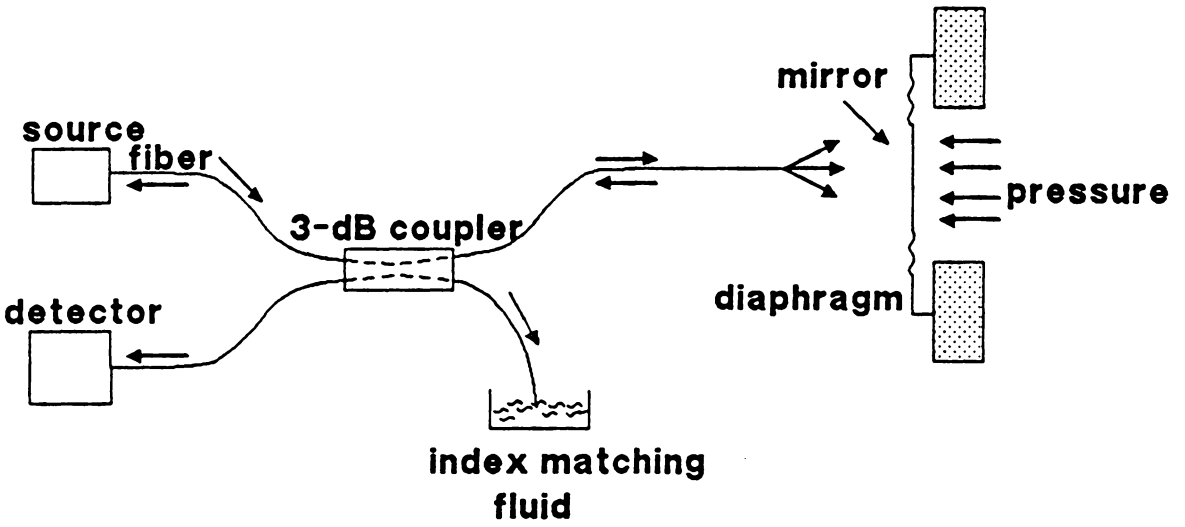

Figure 11. Schematic diagram of a reflection-based pressure sensor with horizontal motion for the reflecting element.

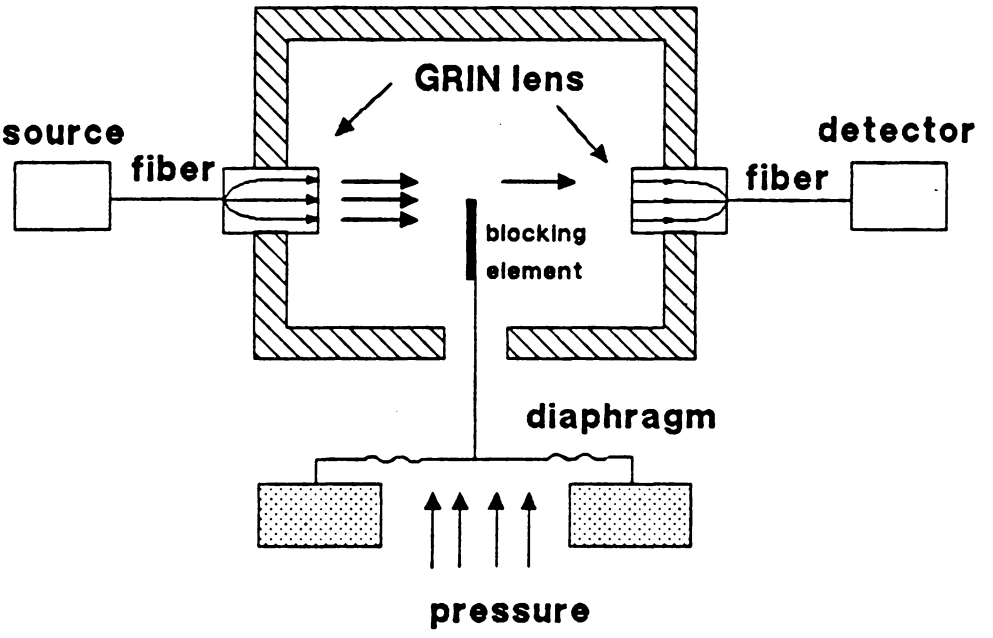

Figure 12. Schematic diagram of a transmission-based pressure sensor.

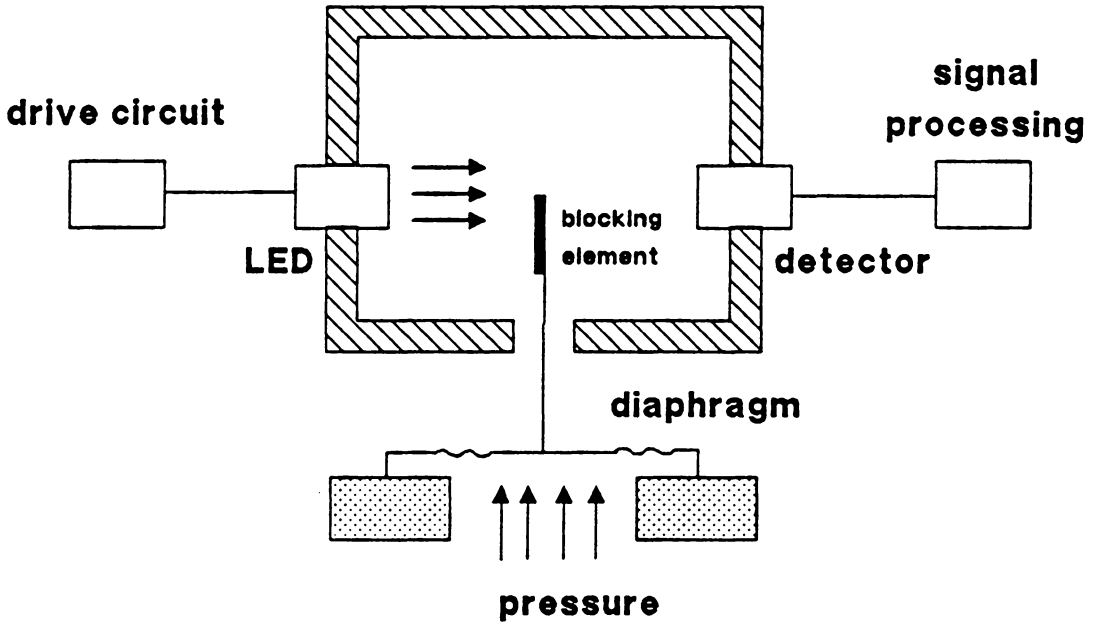

Figure 13. Modified transmission-based pressure sensor without fiber and GRIN lens.

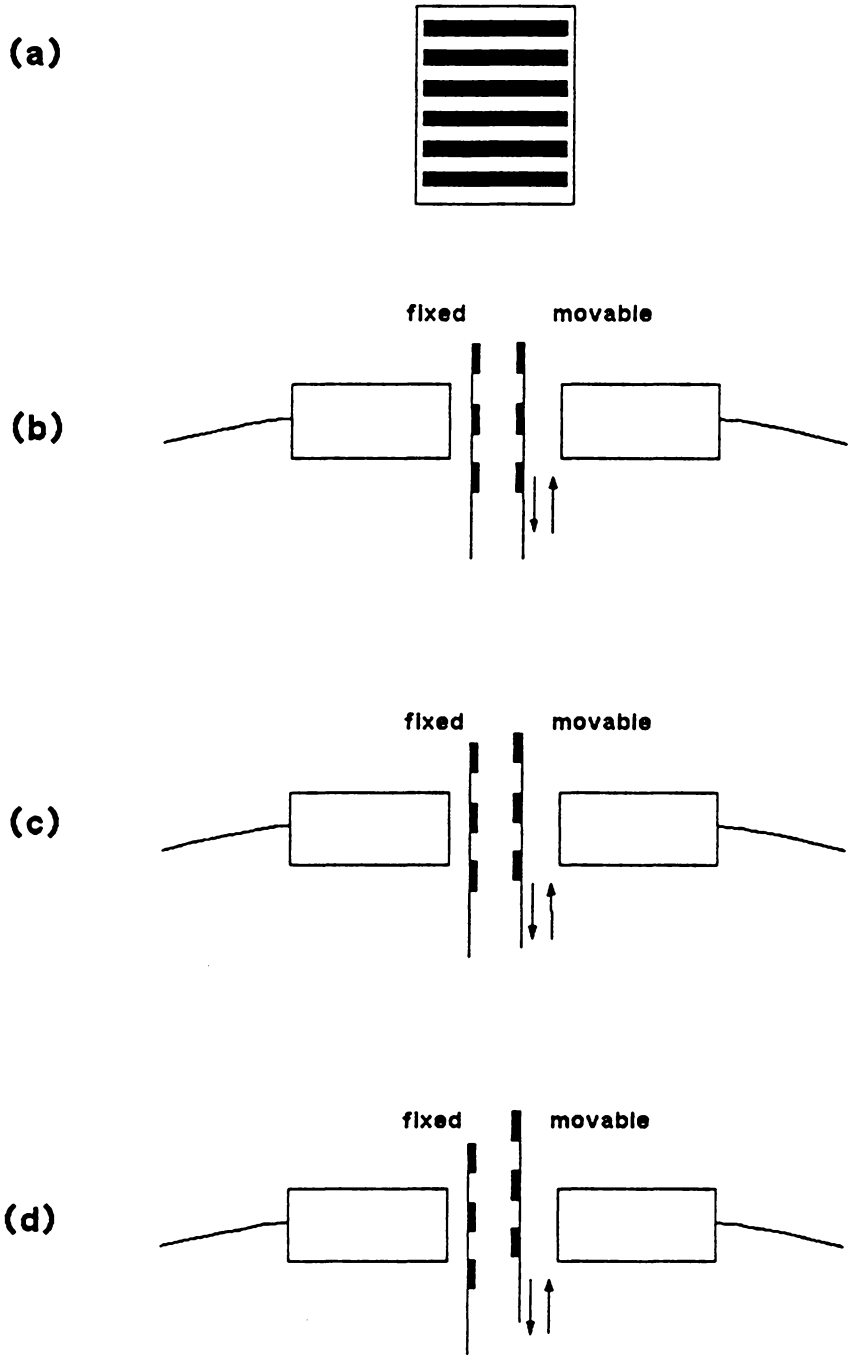

Figure 14. (a) Illustration of sensitivity improvement. (a) gratings. (b) maximum, (c) partial, (d) no transmission.

Chapter 4. Design and evaluation of fiber-optic displacement sensor

A fiber-optic displacement sensor based on the configuration described in Fig. 13 is designed and evaluated. Details of drive circuitry for light source and light detector are given. A micropositioner with a blocking element attached to it is used to simulate the displacement of an actual diaphragm. Variations of the output power versus displacement is calculated and measured. A sensitivity analysis is also carried out.

4.1. Drive circuit for light source

A light emitting diode (LED) is used as the light source. When forward biased, an LED generates light at a specific wavelength. The wavelength of the emitted light depends on the material composition of the active layer in the LED structure. The LED used in the developed sensor is a Honeywell-HFE 4807-015, which emits light at a wavelength $\lambda = 850nm$. The output power increases almost linearly with the input current. A current of 100 mA is recommended by the manufacturer. A simple drive circuit for LED is shown in Fig. 15 [19]. Assuming a turn-on voltage V_γ for the LED, the current I_D flowing in the circuit is obtained from

$$I_D = \frac{V_o - V_\gamma}{R_1 + R_2}. \tag{4.1}$$

The variable resistor R_2 is to allow for the adjustment of current. For $V_o = 15$ V, $V_\gamma = 0.7$ V, $R_1 = 100\ \Omega$, and R_2 varying from 0 to 100 Ω, the current varies in the range 71.5 mA $< I_D <$ 143 mA . An intermediate setting for R_2 provides a current $I_D = 100$ mA .

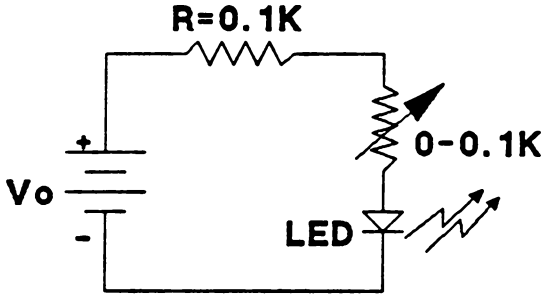

Figure 15. Drive circuit for LED.

4.2. Detection circuit

The light detector is a semiconductor photodiode which converts the light energy into an electrical signal. Here a PIN diode is used as a light detection element. The PIN diode is reversed biased in order to create a strong electric field to separate the released electrons and holes in the intrinsic region. A simple bias circuit is shown in Fig. 16a. The maximum value of R_L of 0.85KΩ is chosen such that the rise time is not increased considerably. Based on the photodiode equivalent circuit shown in Fig. 16b, the rise time is obtained from [20]

$$t_r = 2.19 R_L C_d. \tag{4.2}$$

The photodiode used in the sensor is a Honeywell HFD 3843-002 with the following set of specifications.

$$\lambda = 850\ nm, \qquad \rho = 0.45\ A/W, \qquad I_d = 2.0\ nA,$$
$$t_r = 10\ nsec, \qquad C_d = 1.4\ pF,$$

where λ, ρ, I_d, t_r, and C_d are wavelength, responsivity, dark current, rise time, and detector's junction capacitance, respectively. Substituting for T_r and C_d, $R_L \cong 815\ \Omega$ is obtained.

Another quantity of interest is the minimum detectable power which is obtained as

$$\rho = \frac{I_d}{p} \text{ and, } p = \frac{I_d}{\rho} = \frac{2nA}{0.45\frac{A}{W}} \cong 4.44\ nWatts. \tag{4.3}$$

The minimum detectable power is, in fact, a measure of the minimum measurable weight. The detector output signal is amplified using a two-stage amplifier. Figure 16c

illustrates the diagram of a single stage amplifier. The first stage provides a voltage gain of 50 and the second stage a voltage gain of 20. Thus, a total voltage gain of 1000 can be achieved.

4.3. Evaluation of sensor response

To evaluate the response of the displacement sensor, a set up such as shown in Figs. 12 and 13 are used. A positioner is used to simulate the displacement of the blocking element. Let us assume that light is distributed uniformly over the GRIN lens cross section. Then, the transmitted power is proportional to the unblocked area of the GRIN lens. If x denotes the displacement of the blocking element as indicated in the inset of Fig. 17a, the ratio of the transmitted power to the incident power is

$$\frac{P_t}{P_i} = \frac{S_1}{S_0} = 1 - \frac{S_2}{S_0} \ , \tag{4.4}$$

Where S_2 is the blocked area of the GRIN lens, and is obtained from

$$S_2 = a^2 \cos^{-1}(1 - \frac{x}{a}) - (a - x)\sqrt{2ax - x^2} \tag{4.5}$$

Combining (4.4) and (4.5) and using $S_0 = \pi a^2$,

$$\frac{P_t}{P_i} = 1 + \frac{1}{\pi}\left[(1 - \frac{x}{a})\sqrt{\frac{2x}{a} - \frac{x^2}{a^2}} - \cos^{-1}(1 - \frac{x}{a})\right] \tag{4.6}$$

Figure 17a Illustrates variations of P_t/P_i versus x/a. It is observed that P_t/P_i varies largely linearly with x/a , particularly in the range $0.2 \leq \frac{x}{a} \leq 1.8$. To improve the linearity, it is possible to black out two small crescent portions of GRIN lens area, as

shown in Fig. 17b. To evaluate the response experimentally, the set up shown in Fig. 12 is used. A power meter is used for detector. Experimental data accumulated for transmission-based displacement sensor are tabulated in Table 3. The data collected are in dBm (relative to reference power of 1mW) and tabulated in normalized form. Columns 2,3, and 4 correspond to (1), eqn. 4.6, (2), the experimental data with the cross sectional area of GRIN lens completely exposed, and (3), data with two small crescent portions of GRIN lens area darkened to improve linearity, respectively. Variations of measured normalized transmitted power versus normalized displacement x/a are shown for all three cases in Fig. 17a. In driving eqn. 4.6 it was assumed that power distribution in GRIN lens is uniform, however, experimental data reveal that, power is concentrated more along axis of the GRIN lens and power distribution along the sides are practically zero. Nevertheless, it is observed that the agreement between the calculated and measured results is good. It is also observed that darkening of the two small crescent sides (see Fig. 17b) slightly improves the linearity of response but of course at price of lowering the maximum transmitted power.

4.4. Sensitivity analysis

Using a linear approximation, the relationship between P_t/P_i and x/a can be expressed as

$$P_t = P_i(1 - 0.5\frac{x}{a}). \tag{4.7}$$

The output voltage of the detector circuit is proportional to P_t ; that is,

$$V_{out} = kP_t, \tag{4.8}$$

where k depends on the responsivity of the photodiode and the gain of the amplifier. Combining (4.7) and (4.8), yields

$$V_{out} = kP_t(1 - 0.5\frac{x}{a}). \tag{4.9}$$

Sensitivity is defined as

$$S = \left| \frac{\Delta V_{out}}{\Delta x} \right| = 0.5k\frac{P_t}{a}. \tag{4.10}$$

In eq. (4.10), the GRIN lens radius, a, is fixed. Thus, to increase the sensitivity, the power emitted from the source and/or the gain of the amplifier stage may be increased. As mentioned earlier, the sensitivity may also be increased using a pair of gratings. To illustrate sensitivity improvement, set up of Figs 12 and 13 are used with grating period of about 1mm to detect displacements as small as 0.5mm. The experimental data are tabulated in Table 4 and plotted in Figs. 18 and 19, respectively. Because of large no of data collected, only data for first few cycles are given in Table 4. The variations of detected power in a displacement range of about 1mm and the impact of using grating to improve sensitivity is highlighted in Fig. 20. By observing an increase in slope of response, the utilization of gratings to improve the sensitivity is established. Furthermore, by counting the number of fringes, one can readily determine the displacement very accurately. For the present application an adequate sensitivity is achieved without the use of gratings.

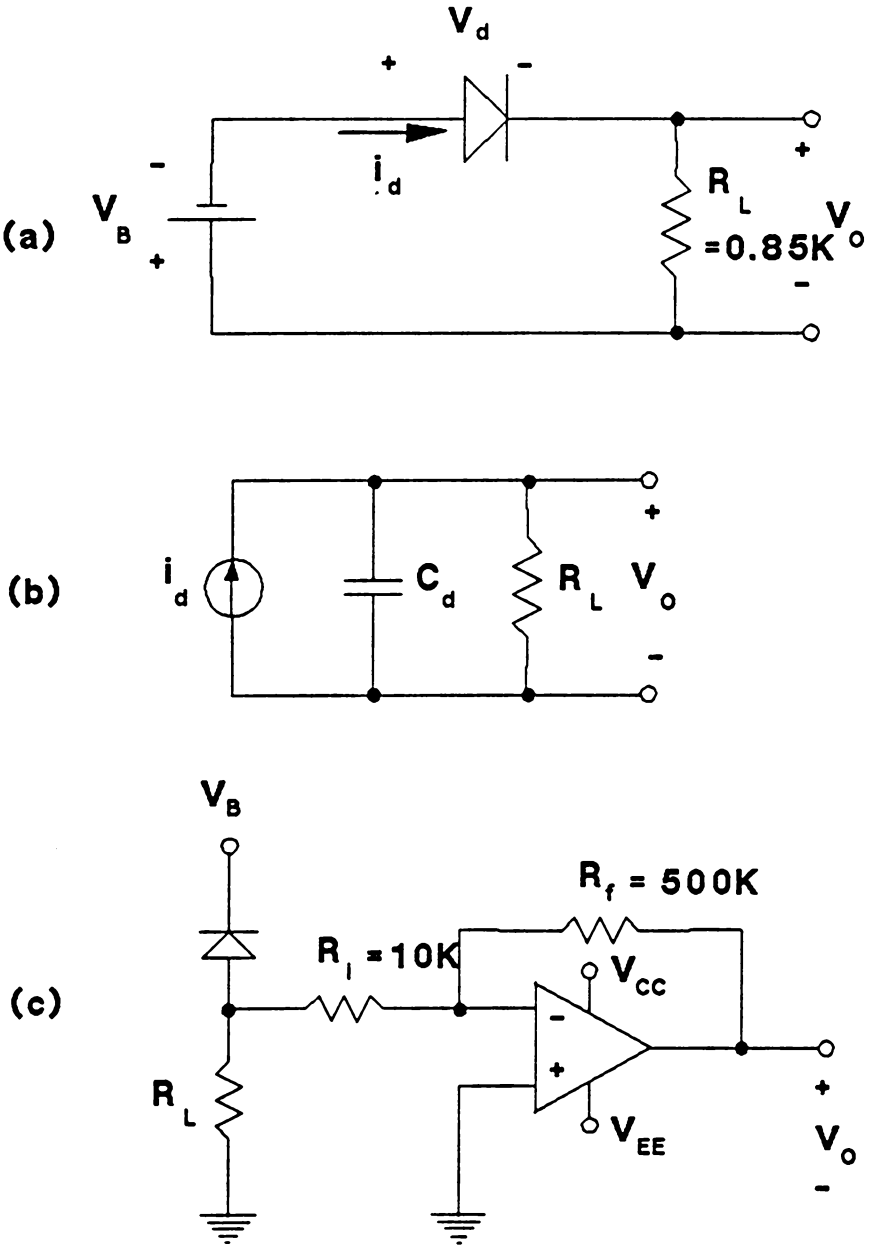

Figure 16. (a) Bias circuit for photodiode, (b) equivalent circuit for photodiode, and (c) amplifier circuit.

Table 3. Experimental data for illustration of improving linearity

Displacement (mm)	$P_t/P_i(1)$	$P_t/P_i(2)$	$P_t/P_i(3)$
0.0	1.0	1.0	1.0
0.2	0.987	1.0	1.0
0.4	0.963	1.0	1.0
0.6	0.932	1.0	1.0
0.8	0.897	1.0	1.0
1.0	0.858	0.977	1.0
1.1	0.837	0.977	1.0
1.2	0.816	0.977	1.0
1.3	0.793	0.955	1.0
1.4	0.771	0.955	1.0
1.5	0.748	0.933	0.977
1.6	0.724	0.891	0.955
1.7	0.700	0.871	0.912
1.8	0.676	0.832	0.871
1.9	0.651	0.794	0.832
2.0	0.627	0.759	0.794
2.1	0.601	0.724	0.741
2.2	0.576	0.661	0.676
2.3	0.551	0.617	0.631
2.4	0.526	0.575	0.575
2.5	0.500	0.513	0.513
2.6	0.475	0.468	0.457
2.7	0.449	0.417	0.407
2.8	0.424	0.363	0.347
2.9	0.399	0.316	0.302
3.0	0.374	0.269	0.251
3.1	0.349	0.229	0.204
3.2	0.324	0.195	0.162
3.3	0.299	0.155	0.126
3.4	0.276	0.126	0.095
3.5	0.252	0.10	0.068
3.6	0.229	0.076	0.045
3.7	0.206	0.059	0.026
3.8	0.185	0.045	0.020
3.9	0.163	0.033	0.019
4.0	0.142	0.026	0.019
4.2	0.103	0.018	0.019
4.4	0.068	0.017	0.018
4.6	0.038	0.017	0.018
4.8	0.013	0.017	0.018
5.0	0.001	0.017	0.018

Table 4. Experimental data for illustration of sensitivity improvement

	with GRIN lens	without GRIN lens
Displacement (mm)	Voltage (V)	Voltage (V)
0.0	7.4	9.8
0.5	7.4	9.8
1.0	7.4	9.8
1.5	7.4	9.8
2.0	7.4	9.6
2.5	7.3	3.6
2.6	7.2	1.6
2.7	7.1	0.6
2.8	7.0	2.3
2.9	6.9	3.6
3.0	6.5	6.0
3.1	5.8	7.6
3.2	5.0	6.9
3.3	4.0	4.7
3.4	2.9	2.6
3.5	1.3	1.0
3.6	0.6	0.9
3.7	0.7	3.1
3.8	2.3	5.4
3.9	4.0	7.7
4.0	5.5	6.0
4.1	7.4	4.7
4.2	4.4	2.4
4.3	2.6	1.0
4.4	0.9	2.0
4.5	0.5	3.8
4.6	1.6	6.0
4.7	3.5	7.6
4.8	5.1	7.2
4.9	7.3	5.5
5.0	4.2	3.3
5.1	2.4	1.5
5.2	0.9	0.8
5.3	0.5	2.2
5.4	2.0	3.6
5.5	3.6	5.9
5.6	5.2	7.7
5.7	7.4	6.2
5.8	4.8	4.4
5.9	3.4	2.4
6.0	2.0	0.8

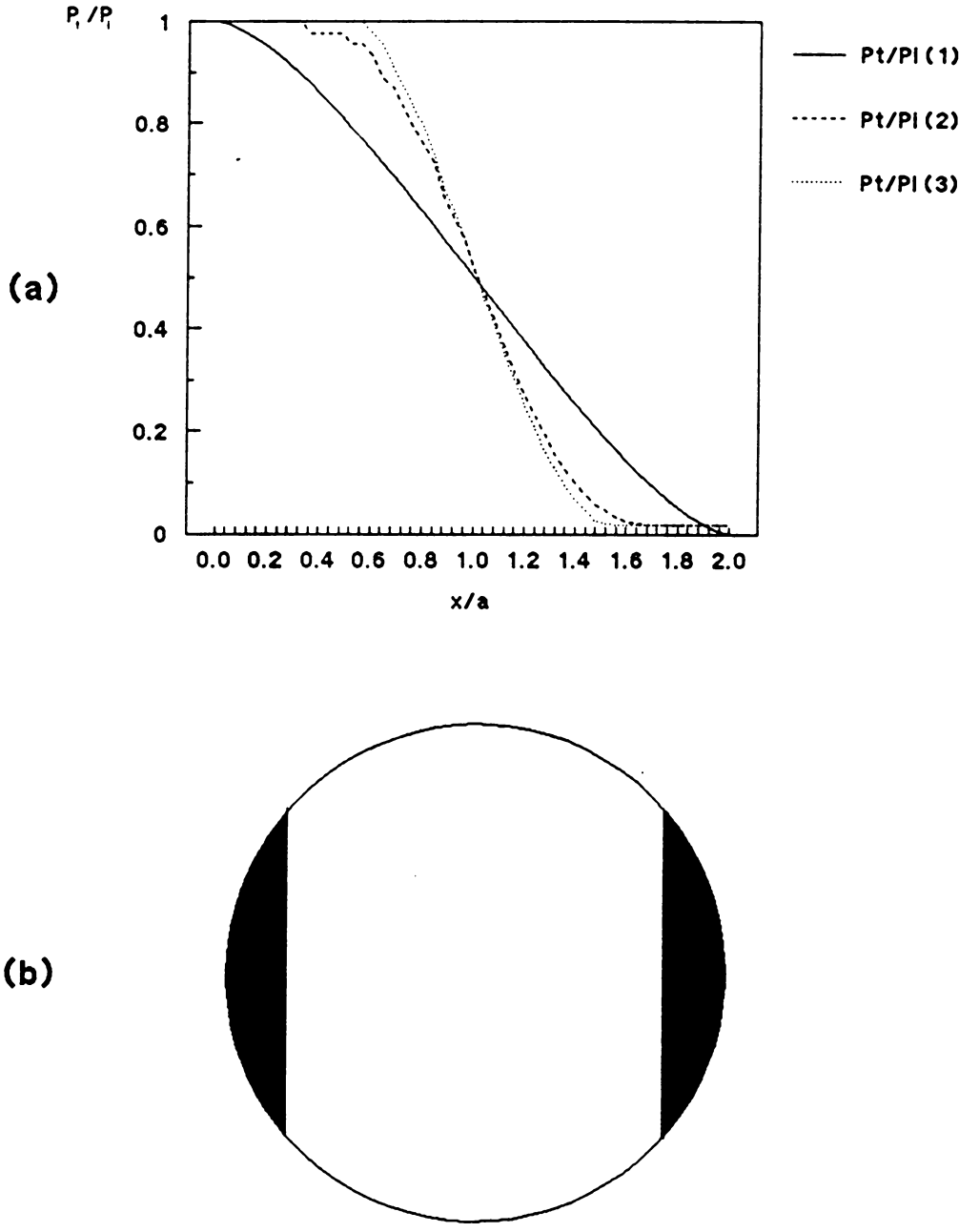

Figure 17. (a) Variations of normalized transmitted power versus normalized displacement and (b) blackened areas improve the linearity.

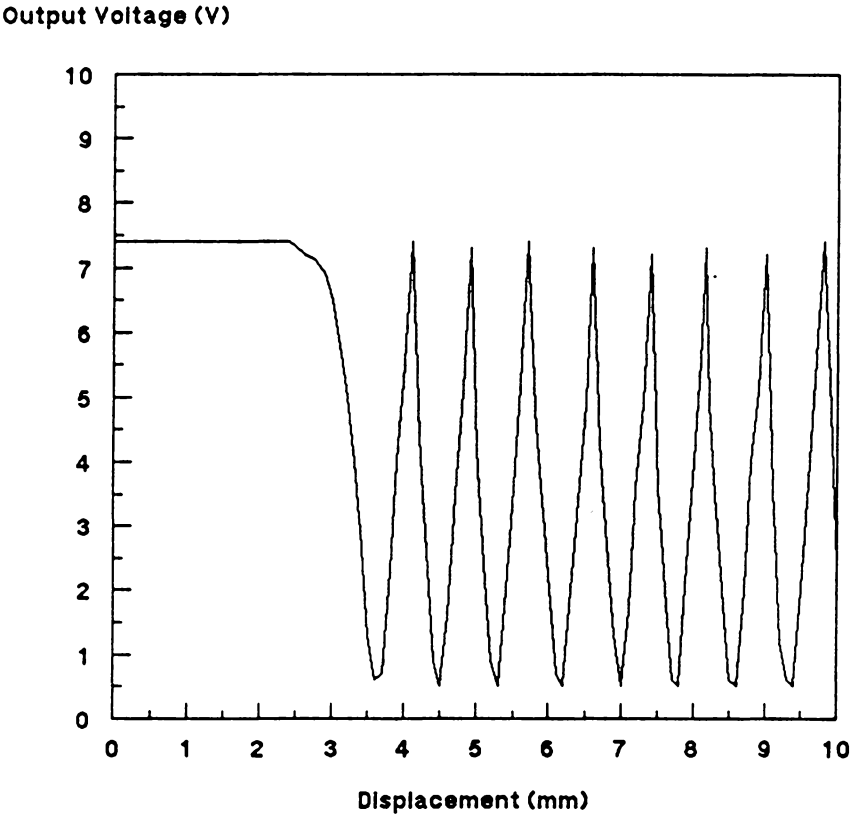

Figure 18. Plot of experimental data for transmission-based pressure sensor with GRIN lens

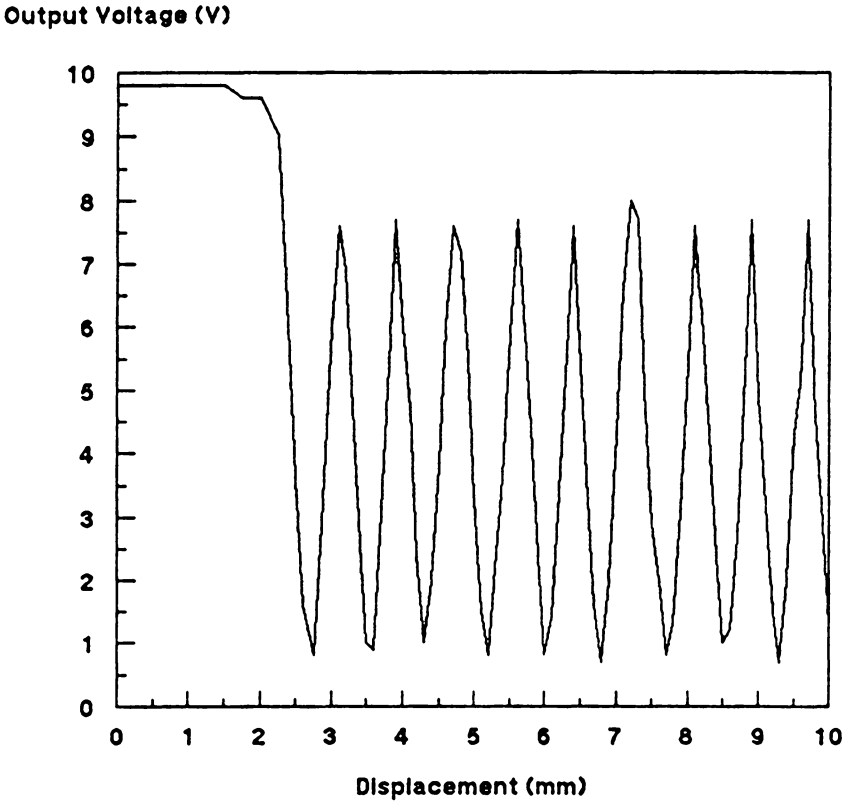

Figure 19. Plot of experimental data for transmission-based pressure sensor without GRIN lens.

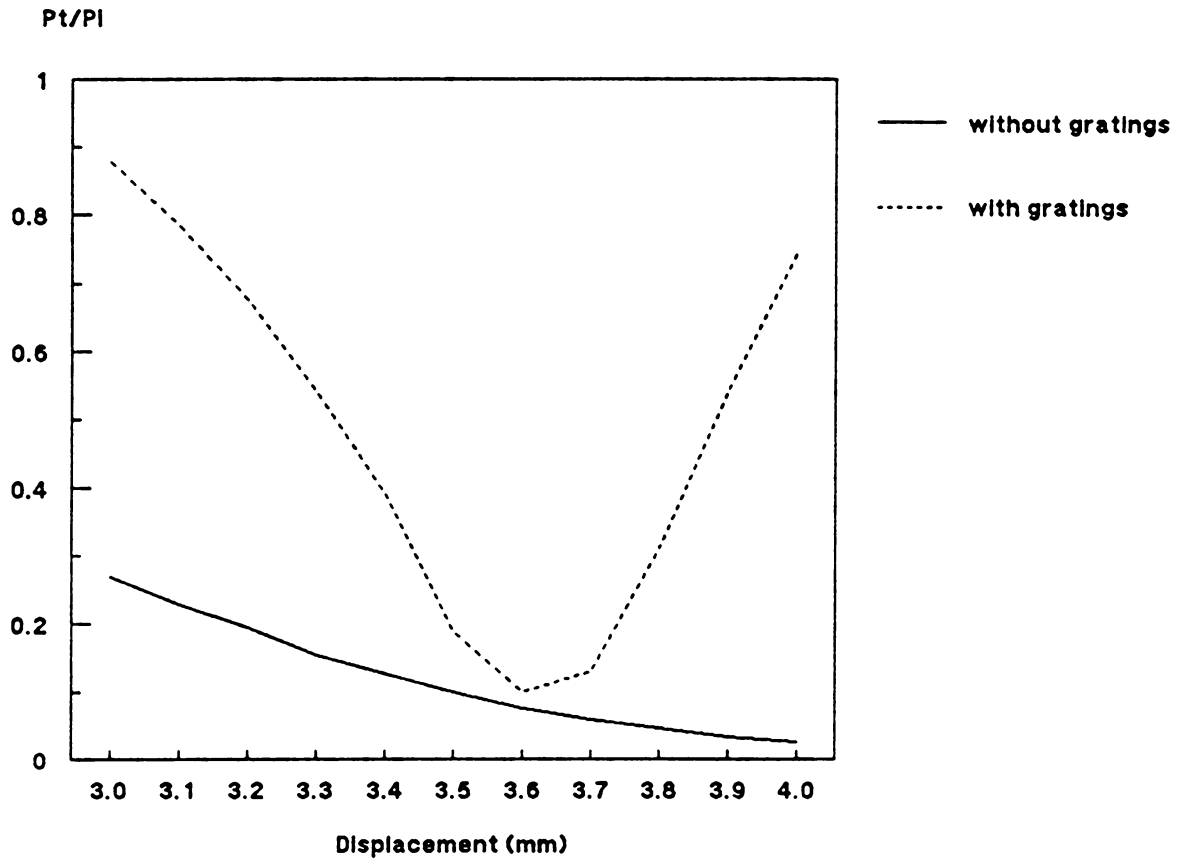

Figure 20. (a) Illustration of increased slope of response when gratings are implemented.

Chapter 5. Experiments with optical pressure sensor

The sensor assembly consisting of an optical displacement sensor, a diaphragm, and a tube filled with an incompressible fluid is described. To evaluate the sensor performance under varying frequencies, a series of experiments using MTS machine to simulate vehicle weights are carried out. The results are analyzed and compared with those of the piezoelectric sensor presented in Chapter 2.

5.1. Sensor assembly

The proposed sensor assembly is schematically shown in Fig. 21. The sensor assembly consists of the following parts:

(a) Optical displacement sensor

This part of the system is an extrinsic fiber-optic displacement sensor with a structure as shown in Fig. 13. Details of operation and performance of such displacement sensor were described in Chapter 4.

(b) Pneumatic tube

The tube is an expandable Master-Flex 6401-15 hose with an inner diameter of 0.25 inches. It is housed in a rubber pad which serves as a mechanical support. The tube is connected at both ends to flexible but non-expandable stainless steel hoses, and is terminated to an air-bleed valve at each end. The longer end hose also transmits the fluid pressure to the diaphragm within the optical sensor assembly. The tube is filled with an incompressible fluid. For laboratory experiments water was used.

(c) Rubber pad

The pad is mainly used for mechanical support and to evenly transmit the applied load to the encased expandable tube. The material composition of the pad is 1618.2 gm of Flexane resin, 4046 cc of Flex-Add, and 355.2 gm of curing agent. It should be noted that the hardness of the rubber pad plays a significant role in the operation of the sensor system. The harder the pad, the greater the amount of loads that can be applied. Mechanical properties of the pad also influence the response of the system both quantitatively and qualitatively. The influence of pad on the output voltage of the optical source, however, can be accommodated through calibration.

(d) Diaphragm

The diaphragm is made of stainless steel and is placed between the optical displacement sensor and the flexible steel hose. The applied pressure causes the diaphragm to deflect. One side of the diaphragm is attached to the light blocking element shown in Fig. 13 in Chapter 3. Thus, the diaphragm converts the pressure into displacement.

(e) Steel hoses and air-bleed valves

Two steel hoses, one 6 feet long and another one foot long, are used. The function of the longer steel hose is to transmit the pressure with minimal loss from the load region to the location of the optical displacement sensor to which the diaphragm is attached. The shorter steel hose is to facilitate the removal of trapped air bubbles. Two air-bleed

valves, one at each end of the pressure sensor assembly, are used to remove any trapped air in the system.

5.2. Experimental set up of the optical sensor assembly

The rubber pad was installed onto the stationary upper plate of an MTS machine. It was firmly supported by four wooden columns along its length, in order to dampen undesired vibrations. Load was applied from below through a metallic support plate. The block diagram of the experimental set up is similar to that of the piezoelectric sensor shown in Fig. 1, Chapter 2.

A 20-Kip MTS machine was used and five levels of load were applied. Each load was applied at different frequencies of 0.25, 0.5, 1, 2.5, 5, and 10 Hz. The applied loads were 0.5, 1, 2, and 3 Kips. When load was increased to 4 Kips, the response saturated due to the buckling of the pneumatic tube. Ten cycles of a square wave were applied at each load-frequency combination (see Table 5). A square wave was used so that the sensor was loaded during half of each cycle. For example, for a load at 1 Hz frequency (1-second period), each cycle is 1 seconds long and the sensor is loaded for 0.5 seconds in each cycle. The MTS was interfaced to an oscilloscope. The input and output signals were monitored simultaneously and photographed following each load application. The output signal of the fiber-optic sensor was obtained for twenty four load-frequency combinations summarized in Table 5. Table 6 summarizes the results of 2-sample t-test performed on the empirical data obtained for all frequencies. The output waveforms were photographed for all cases, but in order to limit the number of figures, only waveforms corresponding to 0.25 Hz, 2.5 Hz, and 10 Hz frequencies are presented here.

Figures 22-25 illustrate these waveforms for loads 0.5, 1, 2, and 3 Kips, respectively. Each figure shows two waveforms; the upper waveform represents the sensor output signal, while the lower one corresponds to the MTS load signal.

5.3. Analysis and discussion of results

Examination of the output waveforms indicates that the initial application of the load induces a voltage which linearly follows the input voltage waveform. A small ringing appears in the output waveform with increased frequency of application, as the rubber pad is relieved of the applied compression. The ringing can be attributed to the oscillation of diaphragm, fluid wave interactions, and the mechanical response time-lag of the rubber pad. The system response is a function of the hardness of the rubber pad which in turn is a function of the material used in fabricating the pad. The harder is the rubber pad, the more sustained will be the oscillations and ringing effects. By properly selecting the incompressible fluid and choosing the right material composition for the pad, these problems can be largely alleviated. Unlike the piezoelectric cable where nonlinearities were evident in the low frequencies of applied loads, for the optical sensor a linear behavior is more clearly demonstrated at lower frequencies as seen in Figs. 22a-25a, which correspond to 0.25 Hz frequency. At this frequency, the load waveform is nearly a square wave, and so is the output waveform. At higher frequencies, e.g., 10 Hz in Figs. 22c-25c, the input waveforms are not clean square waves, but unlike the piezoelectric case the output signals exhibit peaks at instants of application and removal of the load, just as in the case of low frequency loads. In general, however, the variation of the output signal with time for the high frequency loads is more pronounced, but the output waveform still follows the input waveform in a nearly piecewise linear fashion.

Nevertheless, the optical sensor appears to deliver a response less dependent on the frequency of applied loads than does the piezoelectric cable sensor. Statistical analysis are performed to verify the above conclusions and compare the results to those of the piezoelectric cable.

Figure 26 compares variations of the peak-to-peak output voltage versus load at six different frequencies of application. Figure 27 is the best fit regression line through the data. The regression results yield $y = 0.564 + 1.21x$, where y is the output signal in volts and x is the applied load in Kips. The coefficient of determination (R^2) of 91.4% is not significantly different from that of 92.9% in the case of the piezoelectric data. The t-values for the intercept and slope are 3.78 and 15.31, respectively, indicating that both the intercept and slope are significantly different from zero. The corresponding p-values are 0.00102986 and 0.00000000, respectively. The statistically non-zero value of the intercept could stem from attempting to fit a line through an essentially nonlinear data set. The p-values resulted from 2-sample t-tests for both sensors (see Tables 2 and 6) indicate that, frequency dependence of piezoelectric sensor is insignificantly lower since the p-values are higher for the piezoelectric sensor. Tables 2 and 6 also suggest that for level of significance less than or equal to those shown in these tables, the frequency dependence of the sensors from one frequency to the next is insignificant. However, if the level of significance is increased, then dependency on frequency becomes more evident in the case of piezoelectric sensor with generally lower p-values. Of course, the accuracy of these results will increase several folds if the increments of applied load are made smaller and frequency of applied load is changed at smaller intervals. Further examination of the data in Table 6 yields coefficient of variation values of 14%, 16%, 10%, and 6% for applied loads of 0.5, 1, 2, and 3 Kips, respectively. These values are to be compared to those for the piezoelectric sensor, namely 34%, 8%, 20%, and 14%

for 1, 2, 3, and 4 Kips, respectively. Comparison of the two sets of numbers reinforces the earlier conclusion that the fiber-optic sensor output signals are less dependent on the load frequency and thus more accurate. Moreover, Figs. 6, 7, 26, and 27 do indicate that fiber-optic sensor response shows higher linearity of response, thereby the output resulting from the fiber-optic sensor is more apt for further processing.

For loads greater than 3 Kips, the expandable tube buckled and the output signal saturated.

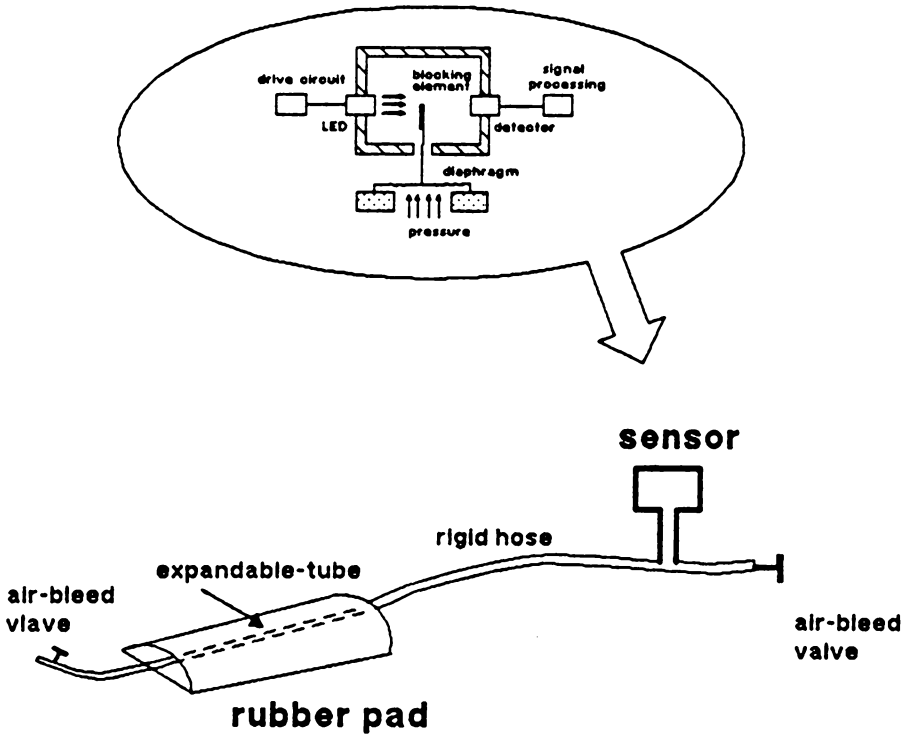

Figure 21. Block diagram of pressure sensor assembly.

(a)

(b)

(c)

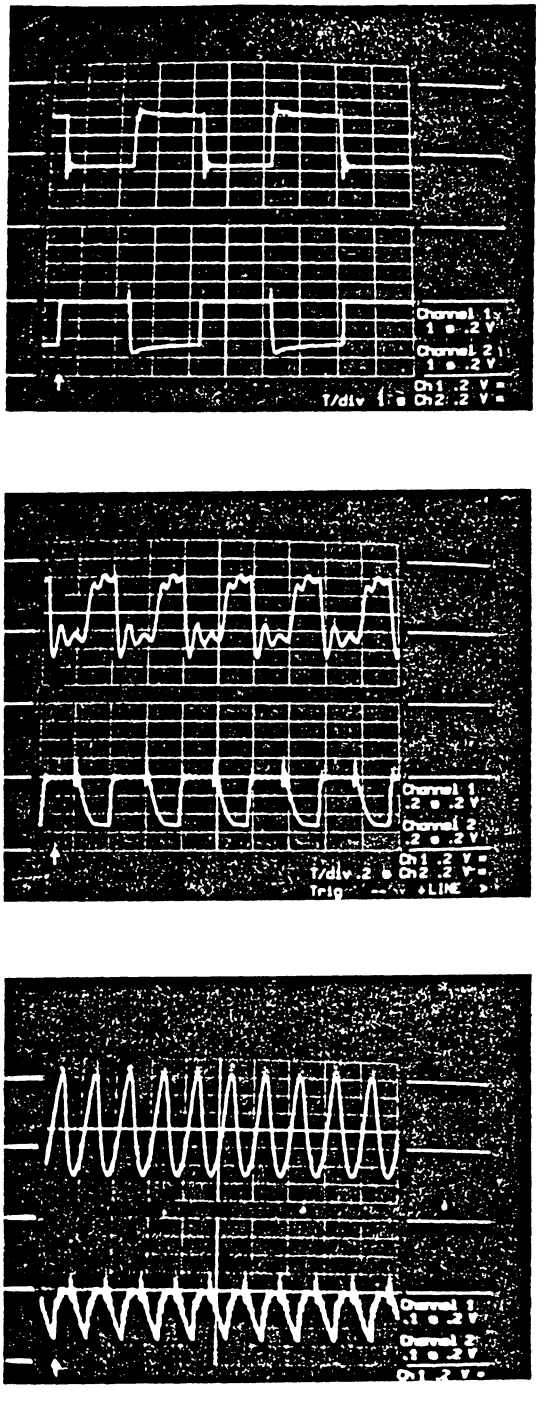

Figure 22. Response of fiber-optic sensor for 0.5 Kips load at frequency (a) 0.25Hz, (b) 2.5 Hz, and (c) 10 Hz.

(a)

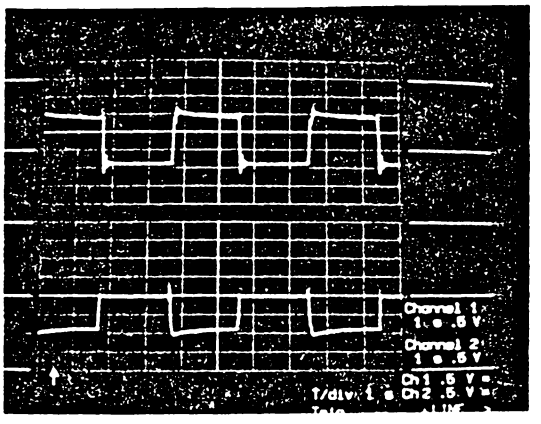

(b)

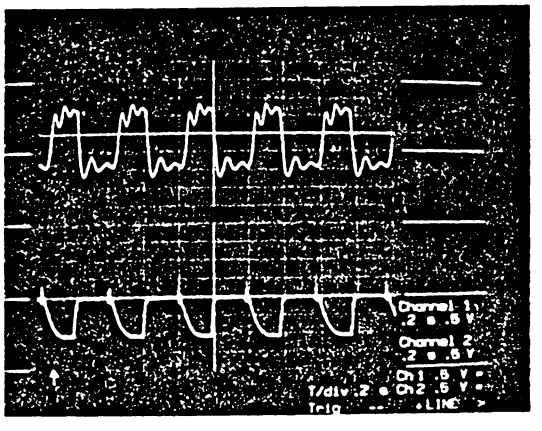

(c)

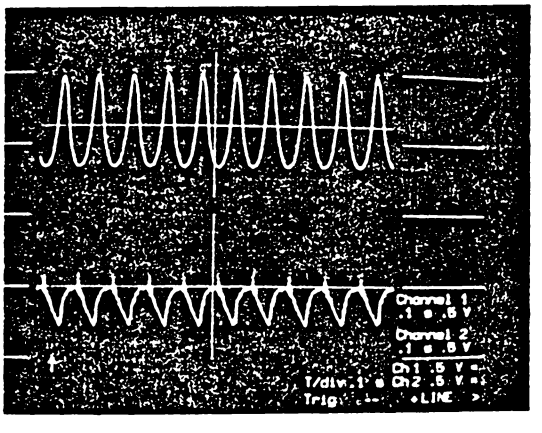

Figure 23. Response of fiber-optic sensor for 1.0 Kip load at frequency (a) 0.25 Hz, (b) 2.5 Hz, and (c) 10 Hz.

(a)

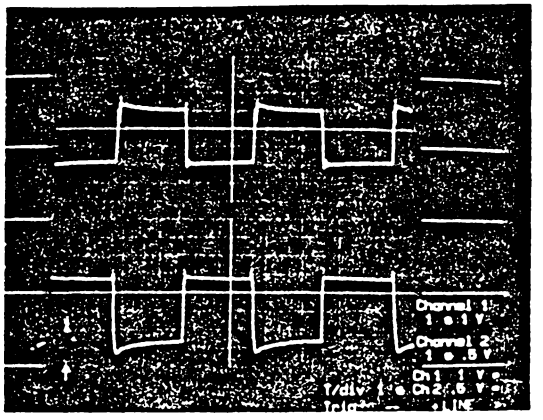

(b)

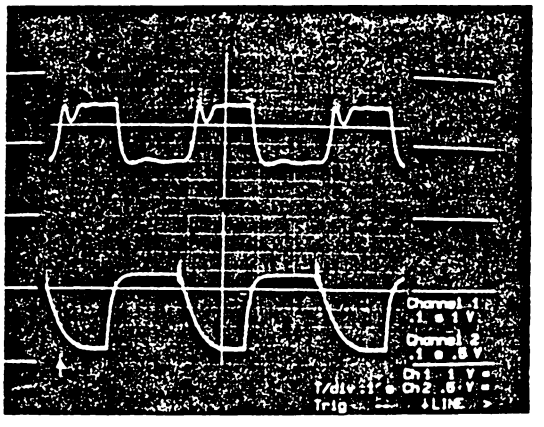

(c)

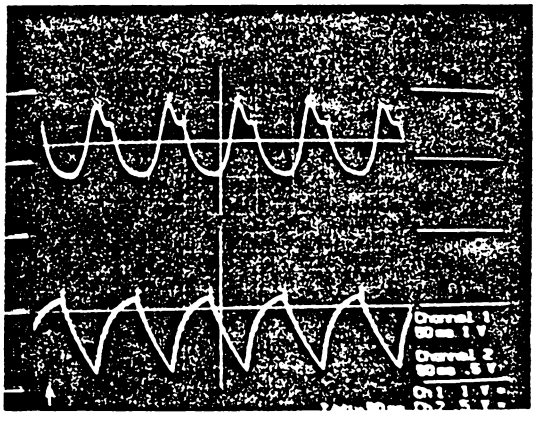

Figure 24. Response of fiber-optic sensor for 2.0 Kips load at frequency (a) 0.25 Hz, (b) 2.5 Hz, (c) 10 Hz.

(a)

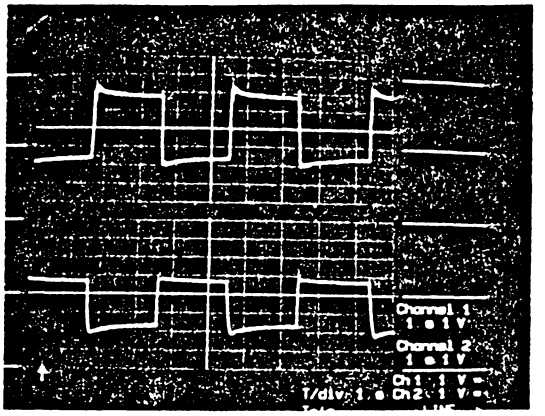

(b)

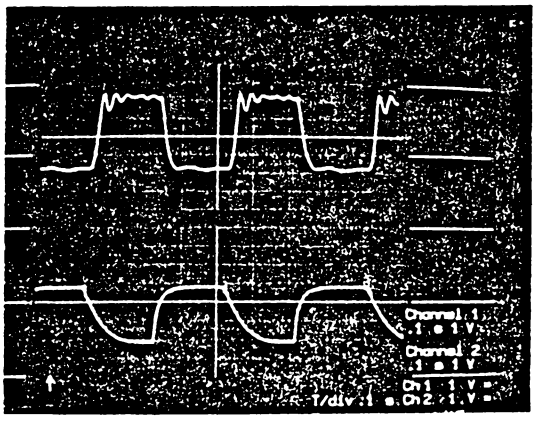

(c)

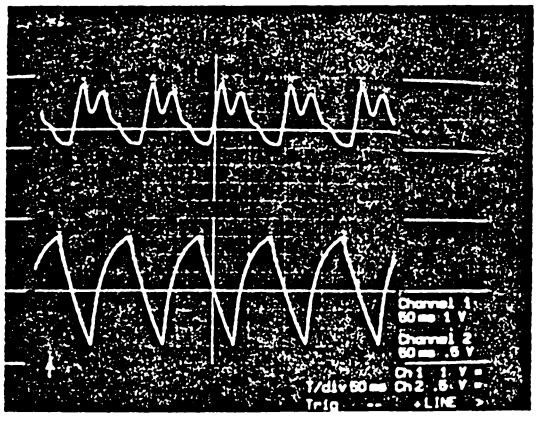

Figure 25. Response of fiber-optic sensor for 3.0 Kips load at frequency (a) 0.25 Hz, (b) 2.5 Hz, and (c) 10 Hz.

Table 5. Experimental data for fiber-optic sensor.

	Induced peak voltage(V) @ Frequency of					
Load(Kips)	0.25 Hz	0.5 Hz	1.0 Hz	2.5 Hz	5.0 Hz	10.0 Hz
0.5	0.7	0.9	0.9	0.9	0.9	1.1
1.0	1.7	1.7	1.7	2.0	2.0	2.5
2.0	3.2	3.2	3.2	3.2	3.2	4.0
3.0	4.0	4.0	4.0	4.1	4.1	3.5
Mean	2.40	2.45	2.45	2.55	2.55	2.78
St. dev	1.48	1.41	1.41	1.40	1.40	1.28

Table 6. p-values for 2-sample t-test on fiber-optic sensor experimental data.

	0.5 Hz	1.0 Hz	2.5 Hz	5.0 Hz	10.0 Hz
0.25 Hz	0.96	0.96	0.89	0.89	0.72
0.5 Hz		1.0	0.92	0.92	0.75
1.0 Hz			0.92	0.92	0.75
2.5 Hz				1.0	0.82
5.0 Hz					0.82

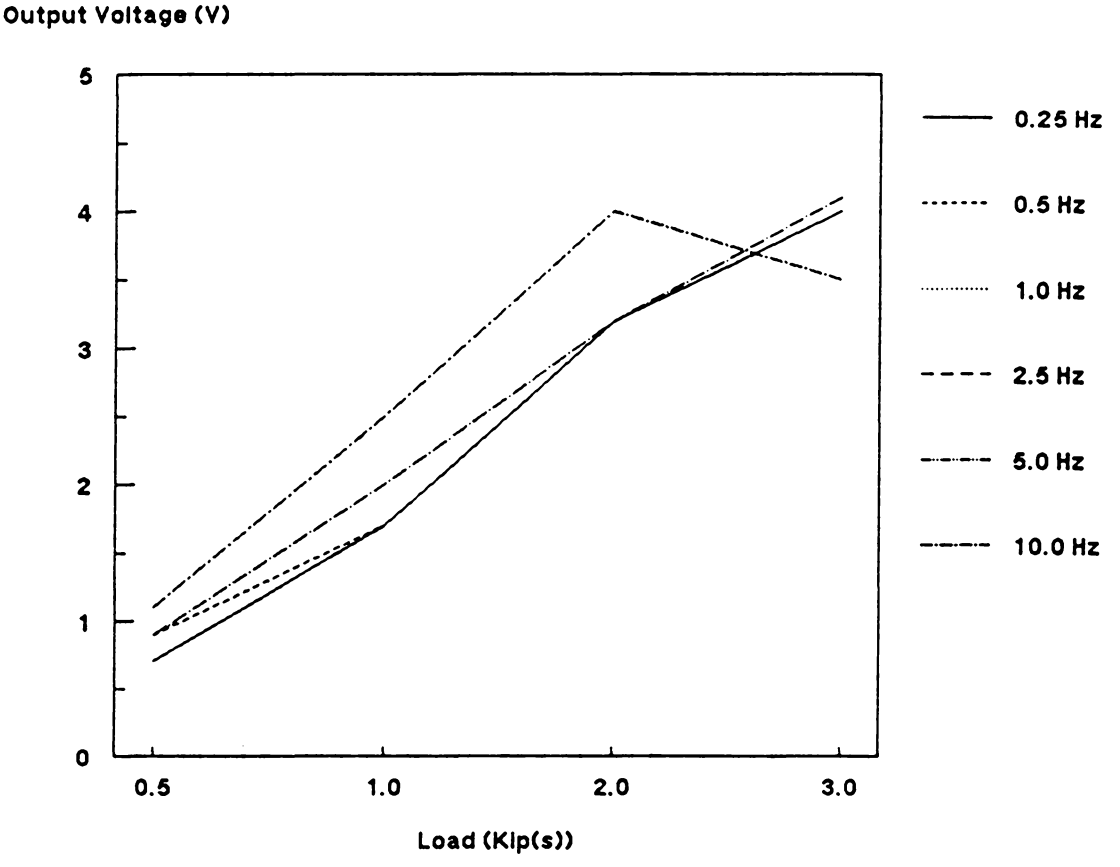

Figure 26. Variations of fiber-optic sensor output voltage with load at different frequencies.

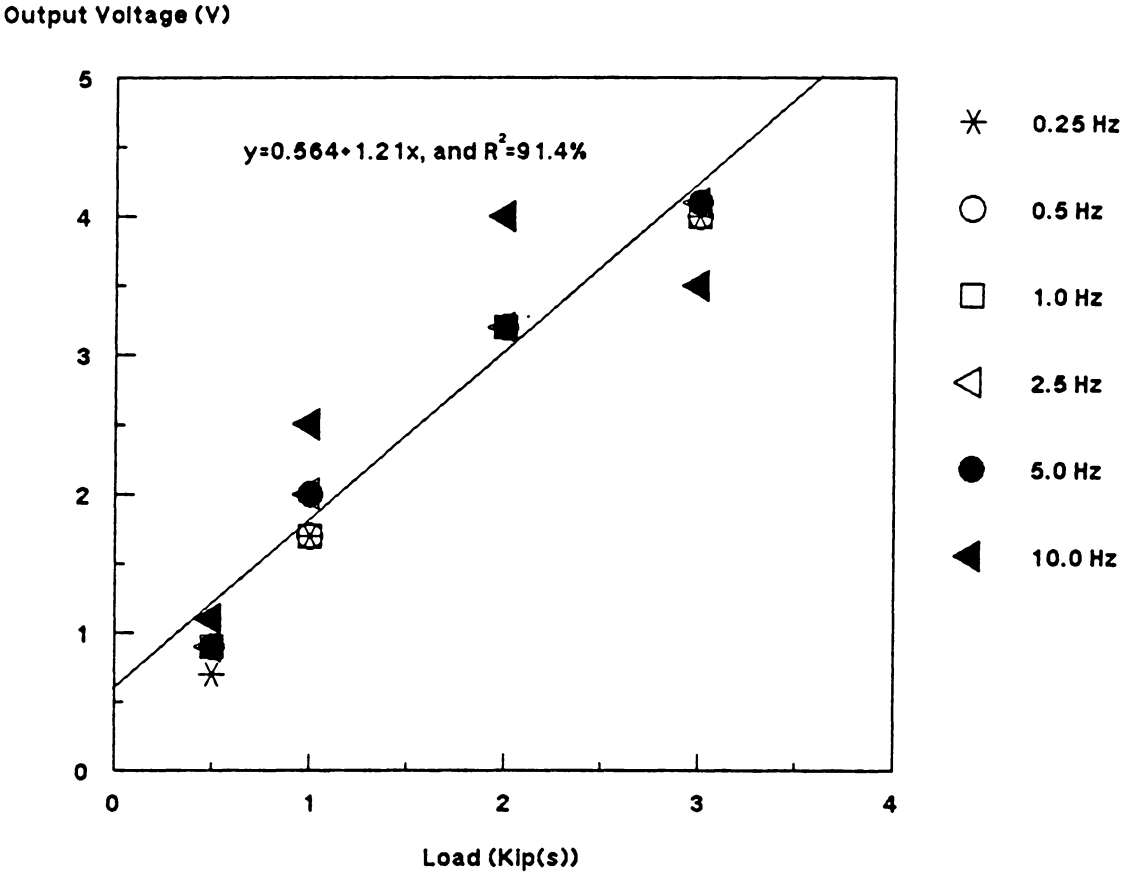

Figure 27. Linear regression of fiber-optic sensor data for varying frequencies of applied load.

Chapter 6. Conclusions and suggestions for further work

The main objective of undertaking this project was to study the feasibility of designing, developing, and implementing a low cost fiber-optic WIM sensor as a possible replacement for piezoelectric WIM sensors. A prototype fiber-optic pressure sensor was designed, manufactured and tested. The sensor consists of a fiber-optic displacement sensor, an expandable hose filled with fluid, an elastomer pad housing the expandable hose, and a stainless steel diaphragm. The prototype sensor was tested under an MTS Loading cell. The performance of the sensor under various loads and different application frequencies was evaluated. Similar tests were performed on a piezoelectric sensor used in WIM systems.

The output signals from each of the two sensors under varying load magnitudes and frequencies were compared. Among the performance attributes considered were: i) the correlation between the applied load and the output voltage signal received, ii) the shape of the output waveforms, and iii) the variation of the output signal with application frequency of the load. In the latter two categories, the optical sensor proved to be superior to the conventional piezoelectric sensor. In the first category, both sensors displayed a fairly linear trend between the magnitude of the output signal and the load applied.

In terms of the shape of the output signal, the piezoelectric sensor generated exponentially decaying output waveforms for square wave inputs. The optical sensor, on the other hand, provided square wave outputs for square wave inputs. In other words, the optical-sensor was reporting a constant voltage reading as long as the MTS loading cell was in contact with the sensor. On the contrary, the piezoelectric sensor output signal would peak to a maximum value proportional to the magnitude of the applied load but would drop back to zero regardless of if or when the load was removed. In signal processing the WIM sensor outputs, the area underneath the output signal wave is a desirable piece of information in determining the axle weights. Therefore, square wave output signals of the fiber-optic sensor offer a significant advantage over the exponentially decaying output waves of the piezoelectric sensor.

Another advantage of the fiber-optic WIM sensor over its piezoelectric counterpart is in output signal variation with load frequency. The data indicate that the signal outputs vary considerably less with load frequency in the case of optical-sensor. Statistical tests establish that the variation of output signals with load frequency for the piezoelectric sensor is slightly less than the optical-sensor case. This is due to readings taken at

applied loading of 3.0 Kips at frequency of 10.0 Hz when the sensor buckled for the case of fiber-optic sensor. The waveforms generated clearly established that the response of fiber-optic sensor is less frequency dependent. This indicates that the speed and axle spacing of vehicles could be a significant source of error in the piezoelectric WIM sensor but not in the fiber-optic case.

The proposed fiber-optic sensor could offer considerably greater accuracy over the piezoelectric sensors. Both the output waveform and the lack of strong frequency dependence in the fiber-optic case greatly contribute to its accuracy. In addition, the fiber-optic signal are not susceptible to electromagnetic interference. Furthermore, unlike the piezoelectric case, the electronic components in the optical sensor are not in direct contact with the wheel, thus they do not undergo permanent deformation and their bending characteristics are not altered. Finally, the optical sensors can be made temperature insensitive. The bending characteristics of the piezoelectric sensors, however, are shown to change at extreme temperatures experienced in the roadway environment.

The optical sensors could also offer a considerably lower life cycle cost. They are portable and are installed over the pavement crown surface. As such they can be installed rapidly and with minimal traffic interruption, especially since there is no need for digging the pavement and embedding the sensor or affixing it to the surface. The electronic components of the optical sensor are cheaper and readily available since they are mass produced for variety of other applications in the fiber-optics and communications fields. The electronic sensor components, which comprise a major fraction of the total sensor cost (over 60%), cost under $600 at time of this writing per sensor unit. Furthermore, the electronic sensor components are installed on the side of

the road and would never be in contact with the traffic, thus lasting longer. The above-mentioned attributes contribute to a lower life cycle cost of the optical sensor as compared to other conventional WIM sensors in use today.

While laboratory tests on the fiber-optics sensor have yielded promising results, the sensor is by no means ready for field implementation. A number of issues must be addressed prior to the implementation phase. The sensor performance characteristics can be optimized through revisions in the design of the various sensor components. The sensor performance needs to be monitored in the field and under actual traffic conditions. Other aspects such as calibration, signal processing, power utilization, and integration into existing vehicle monitoring and classification systems must also be undertaken.

Among the design improvements to be probed is the choice of fluid used to fill the tube to be stretched across the road. The function of the fluid is to transfer the applied pressure to the displacement diaphragm. The transfer of pressure in any fluid medium used must be fairly instantaneous and without much pressure loss. Therefore, a fairly incompressible fluid must be used. The degree of instantaneity required is, of course, a function of how frequently pressure is applied. In the lab tests, water was found to perform satisfactorily for frequencies up to 10 Hz. For the usual range of operating speeds and axle spacings, frequencies exceeding 10 Hz are rarely experienced. The sensitivity of water to temperature, however, makes it unsuitable for field applications. Brake fluid is a potentially good replacement since it is incompressible and considerably less temperature sensitive than water. It is however, not an ideal fluid in case of a ruptured tube and spillage into the pavement surface. The search for the fluid to be used

should also focus on the chemical properties of the fluid, specifically its interaction with pavement materials and its effect on skid resistance characteristics of pavement surface.

The rubber padding must also undergo improvements in design. Specifically, different mix ratios of the Flexane resin and curing agents used in the laboratory prototype must be evaluated. The evaluation criteria should consider those characteristics of the rubber padding desirable under operational field conditions. Among them, the padding must be perfectly elastic for the type of wheel loads expected. Yet, the rubber used must be of a hardness to prevent deflections so great as to completely close off the highly flexible hose embedded in the padding. The shape of the padding should be of concern. A semi-cylindrical padding was used in the laboratory tests. However the bulge introduced on the pavement surface by a semi-cylindrical pad is likely to amplify the undesirable vertical motion of wheels and thus the dynamic loading conditions. The padding to be used in the field must have a thin aerodynamic shape yet be thick enough to provide a suitable cushion for the embedded 0.25-inch diameter flexible hose. Whether or not a smaller diameter inner hose can be used should also be addressed. The latter, however, is a function of the rubber padding. Therefore, an optimum design for field conditions should be reached in terms of the elasticity, hardness, temperature sensitivity, shape, and thickness of the rubber padding as well as the diameter of the inner hose.

Upon design improvements which condition the sensor for field applications, a number of field tests must be conducted. The sensor must be tested for a variety of known axle load and combinations. One possibility is to set up the sensor upstream or downstream of static weigh stations on the highway. This would provide data on a variety of axle configurations and loads. However, it would require coordination with and cooperation of state highway agencies. Furthermore, unless many sites are monitored, not much

variation in speeds can be obtained. An alternative which may prove more advantageous is to conduct the test on proving grounds using one or more trucks of known weight passing over the sensor at different speeds. The truck weight can be easily varied by, for example, using a water tanker and/or sand truck which dumps a known volume of their load after each set of runs.

Another important aspect of field operations is that of lane discrimination. If the tube is stretched across the entire roadway width, then near simultaneous signals can be received from two or more vehicles traveling shoulder-to-shoulder in adjacent lanes. While this may not be critical if only the total individual axle loads were sought, it would be impossible to determine the gross weights or the distribution of axle and vehicle weights by lane.

In making volume counts using pneumatic tubes, lane discrimination is achieved through multi-installation of counter tubes. In a two lane case, for example, depending on the roadway geometry either a separate tube is stretched across each lane or one tube is across the entire roadway width and a second one across the right or the left lane. Multilane installations may not be a feasible approach in the case of proposed optical WIM sensor, since each sensor has an air-bleed valve at each of the two ends. It is therefore difficult, unlike the volume counters, to terminate and clamp down a WIM tube halfway across the pavement area. Alternatives are to modify the design to alleviate the need for two air-bleed valves or devise a mechanism to close down the inner tube at intermediate points so as to only receive signals emanating from a specific lane.

The lane discrimination problem should be studied in conjunction with integrating the optical WIM sensor into the existing vehicle classification systems. The sensors can easily replace axle detectors in the existing classification systems. They also provide an

additional piece of data, namely the axle weight, thus making it unlikely to, for example, classify a six-axle truck as three separate vehicles. On the other hand, the lane discriminator logic of the vehicle classification system can help determine the gross vehicle weights and distribution of axle loads by lane.

Finally, a number of issues in signal processing must be addressed. Given the operational characteristics of the optical displacement sensor, effective means of filtering the noise and amplifying the signal must be devised. Shape, duration, and peak voltage of the signals must be correlated to the axle weight and loading frequency. Necessary calibrations can then be carried out. Efficient means of data transmission and storage must also be developed. Among the factors to be considered are the degree of immunity from electromagnetic interference (EMI) and electromagnetic pulses (EMP), power requirements for signal processing, and degree of compatibility with signal processing and data transmission procedures in the existing vehicle classification and WIM systems.

In short, the proposed fiber-optics displacement sensor is highly promising. Extensive laboratory tests have proved the concept to be operational, and, in comparison to piezoelectric cables, potentially much more accurate. The cost is also considerably lower, namely under $1,000 per complete sensor system as compared to the piezoelectric sensor with a price tag of at least $2,500 per lane. Additional savings are realized in sensor installation, that unlike other WIM sensors, requires no in-pavement installation or surface affixation.

References

1. McCall, B. M., "Status Report of Federal Highway Administration Demonstration Project," Presented at the 66th Annual TRB Meeting, Washington, D.C., January 1987.

2. Concepts, Advantages, and Applications of WIM Systems, National Weigh-In-Motion Conference, U.S. Department of Transportation, Federal Highway Administration, and Colorado Department of Highways, Denver, Colorado, July 11-15, 1983.

3. Al-Rashid, N. I., C. E. Lee and W. P. Dawkins, "A Theoretical and Experimental Study of Dynamic Highway Loading," Report No. 108-1F, Center for Transportation Research, The University of Texas at Austin, 1972.

4. Lee, C. E., B. Izadmehr and R. B. Machemehl, "Demonstration of Weigh-In-Motion Systems for Data Collection and Enforcement," Report No. 557-1F, Center for Transportation Research, The University of Texans at Austin, December 1985.

5. Papagiannkis, A. T., W. A. Phang, J. H. F. Woodrooffe, A. T. Bergen, and R. C. G. Haas, "Accuracy of Weigh-In-Motion Scales and piezoelectric cables," Paper 880449 presented at the 68th Transportation Research Board Meeting, January 1989.

6. Izadmehr, B. and C. E. Lee, "Accuracy and Tolerances of WIM Systems," Presented at the 66th Annual Meeting of Transportation Research Board, Washington, D.C., January 1987.

7. Sommerville, F. and P. Davies, "Low Cost WIM with Piezo Cables," Presented at the 67th Annual Meeting of Transportation Research Board, Washington, D.C., January of 1988.

8. Davies, P., F. K. Sommerville, M. Bettison, and D. R. Salter, Fundamental Properties of Piezo-electric Cable, Report to the Transport and Road Research Laboratory, Phases 1-4, University of Nothingham, 1981-1985.

9. Giallorenzi, T. G., J. A. Bucaro, A. Dandridge, G. H. Siegel, Jr., J. H. Cole, S. C. Rashleigh and R. G. Priest, "Optical Fiber Sensor Technology,"IEEE Journal of Quantum Electronics, Vol. QE-18, April 1982, pp.626-665.

10. Dakin, J. P., "Optical Fiber Sensors; Principles and Applications, "SPIE, Vol. 374, April 1983, pp. 173-183.

11. Culshaw, B., "Optical Fiber Sensing and Signal Processing", Peter Peregrinus Ltd., 1984.

12. Pitt, D. G., P. Extance, R. C. Neet, D. N. Batchelder, R. E. Jones, J. A. Barnett, and R. H. Pratt, "Optical Fiber Sensors," IEE proceedings,

13. Davis, c. M., "Fiber-Optic Sensors: an Overview," Optical Engineering, Vol. 24, March/April 1985, pp. 347-351.

14. McMillan, J. L. and S. C. Robertson, "Single-Mode Optical Fiber Sensors," GEC Journal of Research, Vol. 2, pp. 119-124, 1984.

15. Safaai-Jazi, A., and R. O. Claus, " Synthesis of Interference Patterns in Few-Mode Optical Fibers," SPIE proceedings on Fiber Optic Smart Structures and Skins, Vol. 986, pp. 180-185, 1989.

16. Davies P. and F. K. Sommerville, "Low-Cost WIM: The Way Forward," Presented at the 2nd National WIM Conference, Atlanta, GA, 1985.

17. Auld, B. A., Acoustic Waves in Solids, John Wiley and Sons, New York, 1973, Ch.8.

18. Lagakos, N., P. Macedo, T. Litovitz, R. Mohr, and R. Meister, "Fiber Optic Displacement Sensor," in Physics of Fibers, Vol. 2, Advances in Ceramics , B. Bendow and S. S. Mitra, Eds. Columbus, OH: Amer. Ceramic Society, pp. 539-544, 1981.

19. Personick, S. D., Fiber Optics, Plenum press, New York, 1985, Ch.3.

20. Palais, J. C., Fiber Optics Communications, Prentice-Hall, Englewood Cliffs, 1988, Ch.7.

The vita has been removed from the scanned document